5-2017

Applications of Femtosecond Laser Processed Metallic Surfaces: Leidenfrost Point and Thermal Stability of Rare Earth Oxide Coatings

Anton Charles Hassebrook
University of Nebraska-Lincoln, a.hass.2@hotmail.com

APPLICATIONS OF FEMTOSECOND LASER PROCESSED METALLIC SURFACES: LEIDENFROST POINT AND THERMAL STABILITY OF RARE EARTH OXIDE COATINGS

By

Anton Charles Hassebrook

A THESIS

Presented to the Faculty of

The Graduate College at the University of Nebraska

In Partial Fulfillment of Requirements

For the Degree of Master of Science

Major: Mechanical Engineering and Applied Mechanics

Under the Supervision of Professors Sidy Ndao and George Gogos

Lincoln, Nebraska

May, 2017

APPLICATIONS OF FEMTOSECOND LASER PROCESSED METALLIC SURFACES: LEIDENFROST POINT AND THERMAL STABILITY OF RARE EARTH OXIDE COATINGS

Anton Charles Hassebrook, M.S.

University of Nebraska, 2017

Advisors: Sidy Ndao and George Gogos

In this thesis, micro/nano structured surfaces were created through the use of Femtosecond Laser Surface Processing (FLSP). In the first part of the thesis, an experimental investigation of the effects of droplet diameters and fluid properties on the Leidenfrost temperature of polished and nano/microstructured surfaces has been carried out. Leidenfrost experiments were conducted on a stainless steel 304 polished surface and a stainless steel surface which was processed by a femtosecond laser to form Above Surface Growth (ASG) nano/microstructures. Surface preparation resulted in a root mean square roughness (R_{rms}) of 4.8 μm and 0.04 μm on the laser processed and polished surfaces, respectively. To determine the Leidenfrost temperatures, the droplet lifetime method was employed using Deionized (DI) water and HFE 7300DL. A precision dropper was used to vary the size of DI water droplet diameters from 1.5 to 4 millimeters. The Leidenfrost temperature was shown to display increases as high as 100 °C on the processed surface over the range of droplet sizes, as opposed to a 40 °C increase on the polished surface over the same range of droplet sizes. Average increases of the Leidenfrost temperature between polished and processed samples were as high as 200 °C. The experiment was repeated with HFE 7300DL; however, no noticeable changes of the Leidenfrost temperatures with droplet size were observed, either on the polished or the

processed surface. The difference in the Leidenfrost behavior between DI water and HFE 7300DL and among the various droplet sizes can be attributed to the nature of the force balance and flow hydrodynamics at temperatures slightly below the Leidenfrost point.

In the second part of this thesis, a method of generating nearly superhydrophobic surfaces from FLSP metallic substrates, and a study of their thermal stability at elevated temperatures are presented. Using FLSP, hierarchical micro/nano structures were fabricated on stainless steel 316 after which a 200 nm Cerium Oxide (CeO_2) film was sputtered onto the surface. Before CeO_2 deposition, the contact angle of the sample was measured. Post CeO_2 deposition, the contact angle was measured again. As a result of the CeO_2 deposition, the contact angle of the originally hydrophilic FLSP surface changed to nearly superhydrophobic, with a contact angle of approximately 140^o. Subsequently, the coated surface was annealed in air. The surface maintained its high contact angle from room temperature to about 160^oC, after which it lost its hydrophobicity due to hydrocarbon burn off. For each annealing temperature, the chemical composition for the cerium oxide-coated FLSP surface was monitored using energy dispersive x-ray spectroscopy (EDS) and X-ray diffraction (XRD). Under a nitrogen rich annealing environment, the nearly superhydrophobic FLSP metallic surface maintained its high contact angle up to temperatures as high as 265^oC. To further understand the physics behind the observed phenomenon, we investigated two additional samples of polished stainless steel 310 again coated with 200 nm of CeO_2. Once again, the sample heated in nitrogen showed improved thermal stability over the sample heated in oxygen. Additionally, hydrophobicity loss again occurred at approximately $200^\circ C$ confirming that

hydrocarbon adsorption is the underlying mechanism for hydrophobicity in rare earth oxide ceramics.

ACKNOWLEDGEMENTS

I would like to thank both of my advisors, Dr. Sidy Ndao and Dr. George Gogos. You have taught me an incredible amount about engineering, experiments, heat transfer, fluid mechanics, and life. I would also like to thank our collaborators in the Center for Electro-Optics and Functionalized Surfaces including but not limited to Dr. Dennis Alexander, Dr. Craig Zuhlke, Dr. Troy Anderson, Chris Wilson, Alfred Tsubaki, and Ryan Bell for providing functionalized surfaces for all of my experiments as well as assisting with the writing process. Dr. Jeff Shield, Dr. Mike Lucis, and Edwin Peng in the Nebraska Center for Materials and Nanoscience deserve much credit for assisting with sputtering of samples as well as the frequent and often impromptu EDS, SEM, and XRD sessions. Finally, I would like to thank my lab mates in the Nano and Micro Systems Research Laboratory: Ethan Davis, Mahmoud Elzouka, Henry Ems, Ahmed Hamed, Corey Kruse, and Sarah Wallis. Without your support, advice, and encouragement, I would not be here.

Contents

Table of Figures

Table of Tables

CHAPTER 1

INTRODUCTION

Phase change heat transfer may be the most important physical phenomenon currently utilized by humans [1]. Specifically, boiling and condensation are critical processes in applications such as power generation, cryogenics, thermal management, desalination, and refrigeration. This is due to the relative magnitudes of latent and sensible heat; phase change dictates very large rates of heat transfer at low temperature differences [2]. Moreover, boiling and condensation are processes that are highly susceptible to efficiency enhancements which could reduce energy usage and thus greenhouse gas emissions. As such, a large amount of research has been focused on developing technologies that can meet this potential. Unfortunately, however, minimal advancements have been made in the last 40 years [3]. While significant improvements can be seen in lab settings, they have yet to translate to industry due to surface micro/nanostructure complexity and chemical instability.

Boiling, the changing of liquid to vapor, and condensation, the changing of vapor to liquid, are inverse processes; however, they have some similarities which can be exploited. They both depend upon surface wetting typically quantified through the equilibrium or advancing and receding contact angles, respectively. In the case of boiling, an advantageous surface would be highly wetting, absorbing water through a process called wicking. Condensation, on the other hand is much more complex, and can benefit from the effects of both superhydrophilic (water attracting) and superhydrophobic (water repelling) surfaces. A superhydrophilic surface would attract the liquid phase thus reducing the nucleation barrier required for phase change to occur. On the other hand, a

superhydrophobic surface would easily shed condensate thus opening new surface locations for nucleation to occur directly on the condenser surface, rather than through preexisting condensate. Regardless of whether affinity or aversion to a fluid is advantageous, wettability can be used to predict heat transfer. A surfaces' wettability is affected by both structural and chemical factors [4]; as such, surface engineering for tailored wettability will be central to efforts to improve phase change heat transfer efficiency.

Interactions between liquid and solid are typically described by the equilibrium contact angle. For a structured surface, there are considered to be two stable wetting states; Wenzel, where a droplet fully penetrates a surface micro/nanostructure [5], and Cassie-Baxter, where a droplet will be suspended on top of the structures [6]. In general, the equilibrium contact angle is a relation between the surface energies of the three present interfaces. Consider Figure 1-1 for each droplet it can be seen that three unique interfaces exist: liquid-solid, liquid-vapor, and solid-vapor. The contact angle is derived from a force balance at the three phase line where the edge of the droplet contacts both

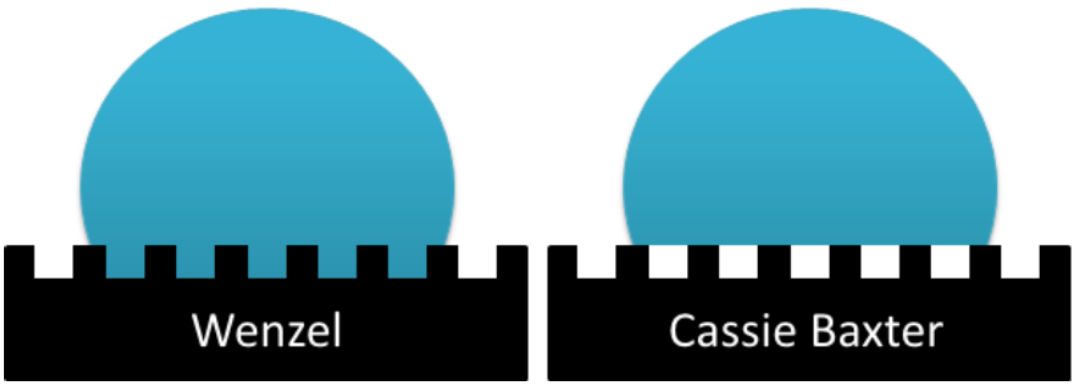

Figure 1-1 Wenzel and Cassie-Baxter wetting states

solid and vapor. For a smooth, chemically homogeneous surface, the equilibrium contact angle can be predicted by Young's equation (1) where γ_{SV}, γ_{SL} , and γ_{LV} represent the solid-vapor, solid-liquid, and liquid-vapor interfacial energies, respectively.

$$\cos\theta_E = \frac{\gamma_{SV} - \gamma_{SL}}{\gamma_{LV}} \quad (1)$$

For a structured surface, the contact angle will be modified depending on the wetting state present. In the case of a Wenzel drop, the equilibrium contact angle is given as

$$\cos\theta^* = r\cos\theta_E \quad (2)$$

In equation (2), r is the roughness factor; this roughness generally modifies the initial wetting properties of a surface. In other words, a hydrophilic surface will become more hydrophilic and a hydrophobic surface will become more hydrophobic. In the case of Cassie-Baxter wetting, the contact angle can be predicted by equation (3).

$$cos\theta^* = r_f f cos\theta_E + f - 1 \quad (3)$$

Here, r_f is the roughness factor of the wetted area, and f is the fraction of solid surface area wet by the liquid. It should be noted that if r_f is equal to r and f =1, then the Cassie-Baxter equation will simplify to the Wenzel equation for a fully wetting liquid.

This thesis is divided into two sections, the first focusing on Leidenfrost boiling, and the second focusing on thermal stability of hydrophobic surfaces. In both sections, polished surfaces were used for control, and the wettability of these surfaces can be reasonably predicted by Young's equation. In chapter 3, the Leidenfrost section, functionalized surfaces were made to be superhydrophilic such that Wenzel wetting was undoubtedly present. In chapter 4, the thermal stability study, the functionalized surfaces showed at times moderate hydrophobicity, and at other times, superhydrophobicity.

Additional work revealed very large hysteresis and roll-off angles for these surfaces indicating that pinning was indeed present and that a true Cassie-Baxter state was likely not.

1.1 Related Literature Review

1.1.1 Effects of Droplet Diameter and Fluid Properties on the Leidenfrost Temperature of Polished and Micro/Nanostructured Surfaces

The Leidenfrost temperature designates the point of minimum heat transfer and the temperature boundary between transition and film boiling. Because the Leidenfrost temperature marks the maximum temperature for efficient heat transfer, it is desirable to have an accurate knowledge and to be able to control the Leidenfrost point (LFP) of a surface. However, in order to manipulate the Leidenfrost temperature, one needs to first understand its governing mechanisms. LFP models based on hypotheses such as hydrodynamic instability, metastable liquid, thermomechanical effects, liquid absorption, cavity activation, and wettability have been previously published in the literature [7–12] and have reasonably explained experimental observations. However, such models do not capture the entire physics, such as the effect of droplet diameter and the balance of the conjugate effects of the various mechanisms when all present.

The Leidenfrost phenomenon on polished surfaces has been extensively investigated. In general, the Leidenfrost state has been found to be governed by surface chemical properties such as surface energy and composition, thermo-physical properties such as density and thermal conductivity, and topographic characteristics of the surface (liquid/solid interface). Many studies have shown the LFP for water on polished stainless

steel to be between 280 and 320 °C [12–18]; such results have been summarized by Bernardin and Mudawar [12] along with the various other LFP models proposed in the literature.

It has been shown that manipulating surface structure and nanoporosity can lead to increased wettability, which in turn will increase the LFP [19–28]. The effects of nanoporosity are believed to be twofold, as a more porous surface will not only have improved wicking for replenishment of dry areas under a releasing vapor bubble, but will also have an increased surface area. Furthermore, because the surface is porous, droplets can be sucked down into the pores, effectively shrinking the vapor layer thickness. A recent publication by Kruse et al. [29], presents large increases, 175 ºC, in the Leidenfrost temperature on stainless steel via functionalized micro/nanostructured surfaces fabricated using Femtosecond Laser Surface Processing (FLSP). These hierarchical surfaces enhance wicking and wettability due to their quasi-periodic, self-assembled, conical microstructures which are coated with a porous layer of nanoparticles. Indeed, the porous layer certainly helps to enhance wicking for replenishment, but as stated earlier, will also artificially shrink the vapor layer by allowing it to exist within the porous network at the surface. Furthermore, overly dense surface structures can decrease the Leidenfrost temperature by impeding escaping vapor, resulting in increased vapor pressure pushing the droplet off the surface in order for vapor to escape [28].

To investigate the effects of the fluid properties, Manzello and Yang [30] found the Leidenfrost temperature of methoxy-nanofluorobutane (HFE 7100) to be 140 °C on a polished stainless steel surface. Meanwhile, Burton et. al. used light interference and high speed imaging to investigate the effects of droplet diameter and substrate temperature on

vapor layer geometry [31]. Their findings show a direct correspondence between the vapor layer thickness, geometry, and droplet diameter. Caswell, using a similar technique, has recently reported a “breathing mode” where the vapor layer thickness under the neck of a droplet rises and falls to allow release of vapor [32]. Caswell found this effect to be independent of droplet diameter, pointing to an underlying instability driven by vapor layer pressure. A few authors [13,33,34] have shown the LFP to be seemingly independent of droplet diameter, while Nishio and Hirata [35] found the LFP to increase with droplet diameter. Specifically, Tamura and Tanasawa [13] showed that Leidenfrost Temperature is independent of droplet diameter for several hydrocarbon fuels. In the present work, we investigate the effects of droplet diameter on the LFP of FLSP and mirror-polished finish stainless steel surfaces using DI water and HFE 7300DL to shed more light onto the effects of droplet size and further understand the mechanisms leading to the Leidenfrost State.

1.1.2 Thermal Stability of Rare Earth Oxide Coated Superhydrophobic Microstructured Metallic Surfaces

Condensation of water vapor is one of the most important natural phenomena used by humans today. A large number of industrial processes such as power generation and refrigeration depend on condensation for operation. Typically, industrial condensers are made from metals such as copper, aluminum, and stainless steel; however, these metals, and their native oxides have very high surface energies resulting in spreading of condensate across the condenser surface. Due to this wetting effect, condensate forms a film (filmwise condensation) which blankets the surface thereby imposing an additional thermal resistance. Conversely, materials that have low surface energy repel water allowing condensate to form and shed as individual drops; this allows for more effective heat transfer between the surface and the vapor. However, materials with low surface energy tend to be nonconductive, which increases the overall thermal resistance of the system, often times erasing any benefit gained from dropwise condensation. It is therefore desirable to create a metallic surface that is superhydrophobic (contact angle >150˚) with low roll off angle (<5˚). To create a superhydrophobic surface on metals, which have a relatively high surface energy, either high surface area structures made of a low surface energy material must be fabricated on the metal surface or the metal must be micro/nanostructured and then coated with a low surface energy material. Several different types of materials have shown promise as hydrophobic coatings including self-assembled monolayers, polymeric materials, noble metals, and rare earth oxides (REO) [36]. It has also been shown that hydrophilic materials can be made superhydrophobic through the use of “doubly reentrant structures” [37,38].

Recently, silanization of surfaces has attracted attention with several researchers [39–41] showing promising results with silane based coatings. These coatings can be made very thin in order to limit thermal resistance while maintaining superhydrophobic nature. This method, however, has not proven to be durable and is therefore not optimal for industrial purposes [42]. To combat durability issues researchers have developed "self-healing" coatings [43,44]. These coatings are based on fluoroalkylsilane which can migrate across a surface to refunctionalize degraded areas. In the case of [43], damaged surfaces with superhydrophilic properties were left in humid air for 4 hours, after which superhydrophobic properties were completely regained. In the case of [44], samples only needed to be heated to 135˚C for 3 minutes to restore superhydrophobicity. Furthermore, their coating showed robust behavior with superhydrophobic properties persisting for 100 cycles.

Polymer coatings [45,46] share many of the features gained from silane coatings such as excellent hydrophobic properties achievable with very low coating thicknesses. However, they also have the same challenges, namely a compromise between coating thickness, thermal resistance, and durability. Paxson et. al. [42] used Initiated Chemical Vapor Deposition (iCVD) to create a poly-(perfluorodecyl acrylate)-co-divinyl benzene (p(PFDA-co-DVB)) grafted polymer coating which maintained dropwise condensation in an accelerated endurance test for 48 hours. They compared their results to a siloxane based coating which degenerated to filmwise condensation in only 30 minutes.

Noble metals have also been used to create hydrophobic coatings [47–49], and have shown sustained dropwise condensation. However, these materials are intrinsically hydrophilic, and thus depend on surface contamination such as hydrocarbons in the

ambient air that adsorb onto the surface of the metals in order to reduce their surface energy. One particular study reported a gold surface maintaining dropwise condensation for up to five years in a closed environment [47]; however, gold and other noble metals are far too expensive for this approach to be economically feasible.

One recently reported method for decreasing surface energy of a metallic substrate used ceramic coating made up of the intrinsically hydrophobic lanthanide series oxides [50]. The authors attributed the hydrophobicity of these rare earth oxide ceramics to their unique electron structure, arguing that "the unfilled 4f orbitals are shielded from interactions with the surrounding environment by the full octet of electrons in the $5s^2p^6$ outer shell". Contact angle measurements showed hydrophobic behavior with measured angles ranging from 100˚ to 110˚; additionally, surfaces coated with these ceramics exhibited dropwise condensation. It was noted however, that when the ceramic coatings were placed in a high temperature, abrasive environment, that hydrophobic properties were lost. This was attributed to destruction of the fragile surface features and delamination of the ceramic coating. In another study [51], it was found that lanthanide series ceramics are not intrinsically hydrophobic as previously thought, but rather adsorb hydrocarbons from ambient air in order to minimize their free surface energy. By monitoring carbon content in relation to contact angle, it was shown that perfectly clean REO surfaces are superhydrophilic (contact angle ~ 0˚), with contact angle increasing proportionally to surface carbon content. While REO surfaces are dependent upon hydrocarbon contamination in the same matter as the previously discussed noble metal coatings, the authors did note some advantages over the currently used technology. When compared to polymer coatings, REO's have significantly increased thermal conductivity.

This allows for much thicker coatings to be applied without significant increase to thermal resistance, which could help to combat durability issues like delamination. Furthermore, when compared to noble metals, REO's are very cheap, so integrating them with current facilities would have a significantly decreased initial investment.

Consequentially, REO's show much promise as coating materials for condensers; however, studies on their heat transfer performance and durability are nonexistent. Therefore, the purpose of this work was to evaluate the thermal stability of hydrophobic and superhydrophobic REO coatings on stainless steel. This was accomplished by monitoring the contact angle of a flat mirror-polished and micro/nanoscale roughened test surface while they underwent cyclic heat treatments.

CHAPTER 2

FEMTOSECOND LASER SURFACE PROCESSING

2.1 Micro/Nanoscale Structure Fabrication

Surface micro/nanostructure has been shown to strongly affect the wettability of a surface which in turn can predict enhancements or impediments in heat transfer. Multi scale surfaces are often to be biologically inspired due to the natural occurrence of such surfaces. Many plants and animals utilize these surfaces for enhanced wettability applications. For example, the Darkling Beetle found in the Namib Desert has evolved a natural condensing surface with mixed areas of superhydrophilicity and superhydrophobicity [52,53]. These mixed areas not only enhance the rate at which water can condense on the beetle's shell, but also direct condensed water to the mouth of the beetle. These biomimetic surfaces are considered to be hierarchical due to the presence of both micro and nanoscale features, both of which contribute significantly to the wettability and heat transfer performance.

In order to fabricate surfaces with tailored wettability, FLSP was used to produce micro/nanoscale features on SS 304. A superhydrophilic surface can be created via a combination of the inherently high surface energy steel and modification of the surface profile by generating microscale structures covered with nanoscale particles. No external coatings or materials were applied to the steel surfaces to obtain the desired structures; the femtosecond laser pulses directly induced modification of the surface. The generation of these surface features is achieved through multi-pulse illumination of the sample using laser fluence values above the material ablation threshold. During FLSP, absorption of laser energy initiates a complex combination of multiple self-organized growth

mechanisms including laser ablation, capillary flow of laser-induced melt layers, and redeposition of ablated material [54–61]. The size and shape of the features are controlled through fabrication parameters including the laser fluence, the number of laser pulses per area incident on the sample, the laser incident angle, and the atmosphere during processing. Furthermore, surface features induced by one laser pulse affect the absorption of light from subsequent pulses, which results in feedback during formation. The surfaces used in this thesis consist of structures that have been termed below surface growth (BSG) and above surface growth (ASG) mounds [29,54]. Scanning electron microscope images of these surface structures can be seen in Figure 2-1, and a visual aid for the formation process can be seen in Figure 2-2. Typically, BSG-mounds are formed using a lower fluence and higher pulse count than ASG-mounds. The beginning

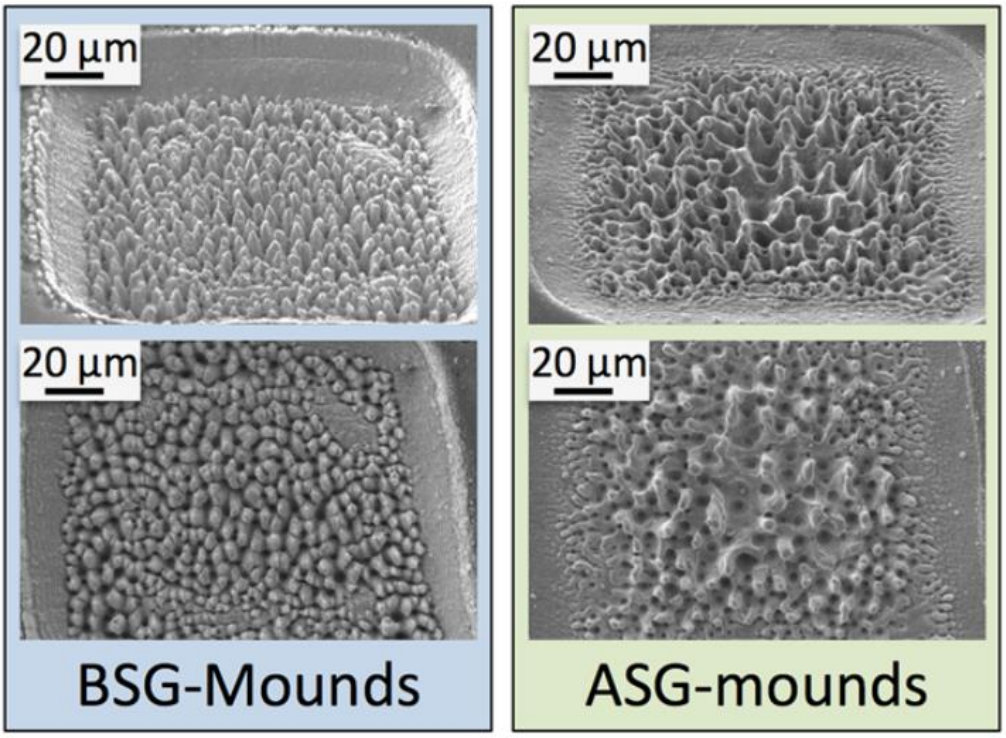

Figure 2-1 Scanning electron microscope images of BSG- and ASG-mounds.

formation processes are very similar for ASG- and BSG-mounds. Phase 1 in Figure 2-2 is dominated by ablation of the surface due to incident laser energy. During this phase, with each incident pulse, the surface microstructure is blasted away and replaced with a new, random structure. This leads to the formation of defects called precursor sites. These precursor sites lead directly into the second phase where laser energy is diffracted to the valleys of the surface causing preferential valley ablation (PVA). For BSG-mounds, the concentrated energy adsorption leads to increased rates of ablation. As material is ablated away, nanoscale particles form in the air above the surface. These nanoparticles readily oxidize and cool, and many of them condense on the surface. For ASG-mounds, the incident energy is enough to cause local melting of the surface, which in turn leads to capillary induced fluid flow. This fluid flow is surface tension driven and is thus sensitive to local temperature gradients on the surface. As a result, molten material typically flows

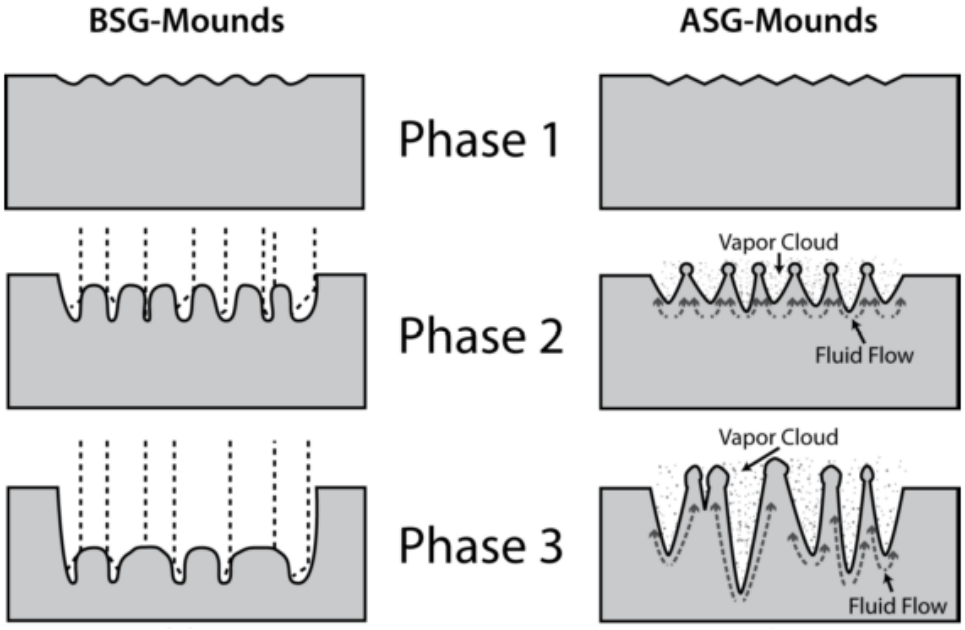

Figure 2-2 FLSP structure formation mechanisms [54]

to the peaks of the mound structures where it forms a porous layer with a mixture of solidified melt and redeposited nanoparticles. For BSG-mounds, the third phase is a continuation of the second, where ablated materials continue to oxidize and condense on the surface. This continued condensation results in further growth of mounds, and in some cases, merging of adjacent mounds. Further detail regarding FLSP processes can be found in the references [54,55,59,60,62].

2.2 Leidenfrost Surface Fabrication Specifics

A single FLSP surface consisting of ASG-Mounds was used for the Leidenfrost study. The laser used to produce the functionalized sample was a Spectra Physics Spitfire, Ti:Sapphire femtosecond laser system (Figure 2-3), which was capable of producing 1 mJ, 50 fs pulses, with a center wavelength of 800 nm. The pulse length and chirp were monitored using a Frequency Resolved Optical Gating (FROG) instrument. The position of the sample with respect to the laser focal volume was controlled using computer-guided Melles Griot nanomotion translation stages with three axes of motion. The laser power was controlled using a half-waveplate and a polarizer. All surface processing was completed in open atmosphere [54]. Material composition analysis of the

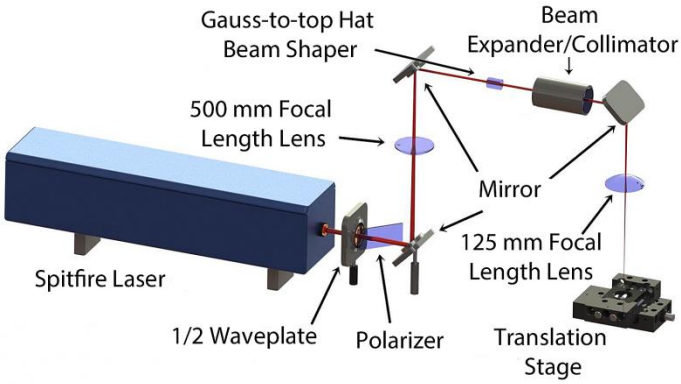

Figure 2-3 Femtosecond laser surface processing setup.

processed sample revealed traces of oxygen which have been attributed to surface oxidation. It should be noted that in a previous study on a sample processed in a similar manner to the sample discussed in this paper, no foreign materials (materials not native to the substrate) were detected in the nanoparticle layer [55].

A square-shaped flat-top beam profile with 150 μm sides was used in order to maintain uniform laser fluence on the material surface during processing. Figure 2-4(A) contains a representative square-shaped flat-top beam profile taken using a WinCamD beam profiler. This beam profile was created using a refractive beam shaper. The laser fluence varied by less than 20% across the central portion of the beam; any fluence fluctuations in the flat-top distribution are attributed to the asymmetries and inhomogeneity of the input beam [54]. In order to process large areas (1.5x1.5 inches), the sample was translated relative to the focal volume in a raster scan pattern as

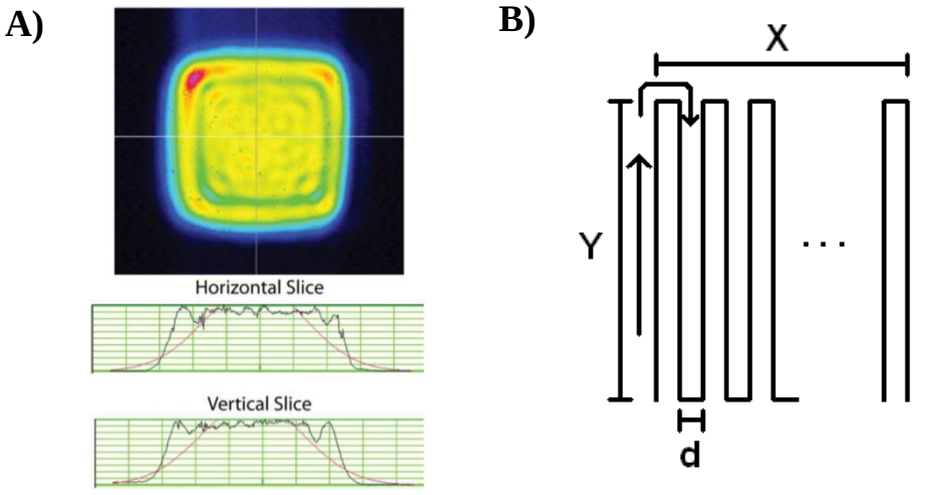

Figure 2-4 (A) Square flat top beam profile of Femtosecond laser pulses. (B) Laser raster pattern. X and Y were approximately 1.5 inches while d was 15μm.

diagramed in Figure 2-4(B). In the Leidenfrost study (chapter 3), the target sample was processed with a laser fluence of 1.4 J/cm^2 and translated at a speed such that the number of incident pulses per spot was 1462.

2.3 Rare Earth Oxide Surface Fabrication Specifics

The surfaces in chapter 4 were fabricated with the same Spectra Physics Spitfire, Ti:Sapphire femtosecond laser system described in section 2.2 (Figure 2-3). However, for the superhydrophobic samples, the flat top beam shaper optics were removed from the FLSP setup, such that the focused pulses had a Gaussian spatial profile. The Gaussian pulses were focused onto the sample surface using a 125 mm focal length plano-convex lens. All surface processing was completed in open atmosphere. In the thermal stability study (chapter 4), the target samples were processed using a peak pulse fluence of 2.20 J/cm^2 and translated at a speed such that the number of incident pulses per spot was 456.

Prior to processing, test surfaces were fabricated by cutting one square inch pieces of stainless steel 316 and prepared with increasingly fine grit sandpaper and buffing compound until a mirror-finish had been achieved. Surfaces were then cleaned via a multistep process. Samples were rinsed with acetone followed by a 20 minute ultrasonic bath in distilled water. Samples were then dried with compressed air and cleaned with a frozen CO_2 sprayer. Finally, the samples were ultrasonically cleaned for 20 minutes in distilled water and dried with compressed air. After FLSP, samples were sputtered with 200 nm cerium oxide.

CHAPTER 3

Effects of Droplet Diameter and Fluid Properties on the Leidenfrost Temperature of Polished and Micro/Nanostructured Surfaces

3.1 Leidenfrost Surface Characterization

Characterization of the FLSP and mirror-polished surfaces was carried out using Scanning Electron Microscope (SEM) images and 3D profilometry scans (Figure 3-1). 3D profilometry scans were taken with a Keyence 3D confocal laser scanning microscope. As can be seen from the figure, the FLSP surface consists of self-assembled microstructures characterized by deep holes separating pointed structures also known as Above Surface Growth Mounds (ASG-Mounds) [54]. Even though it is not shown on the SEM image, ASG-Mounds are covered by a porous layer of nanoparticles which have been previously shown to promote capillary wicking [29,55]. From the 3D confocal laser scanning microscope data, surface roughness and microstructures height information could be obtained: microstructures on the processed surface had an average peak-to-valley height of 24.9 μm and a surface roughness R_{rms} value of 4.8 μm while the polished surface had a measured R_{rms} value of 0.04 μm. Contact angle measurements were carried out using a Ramé-Hart Goniometer and Tensiometer. All measurements were done via the static droplet method with 1 μL droplets of ASTM Type II Deionized water and 3M Novec 7300DL Engineered Fluid (HFE 7300DL).

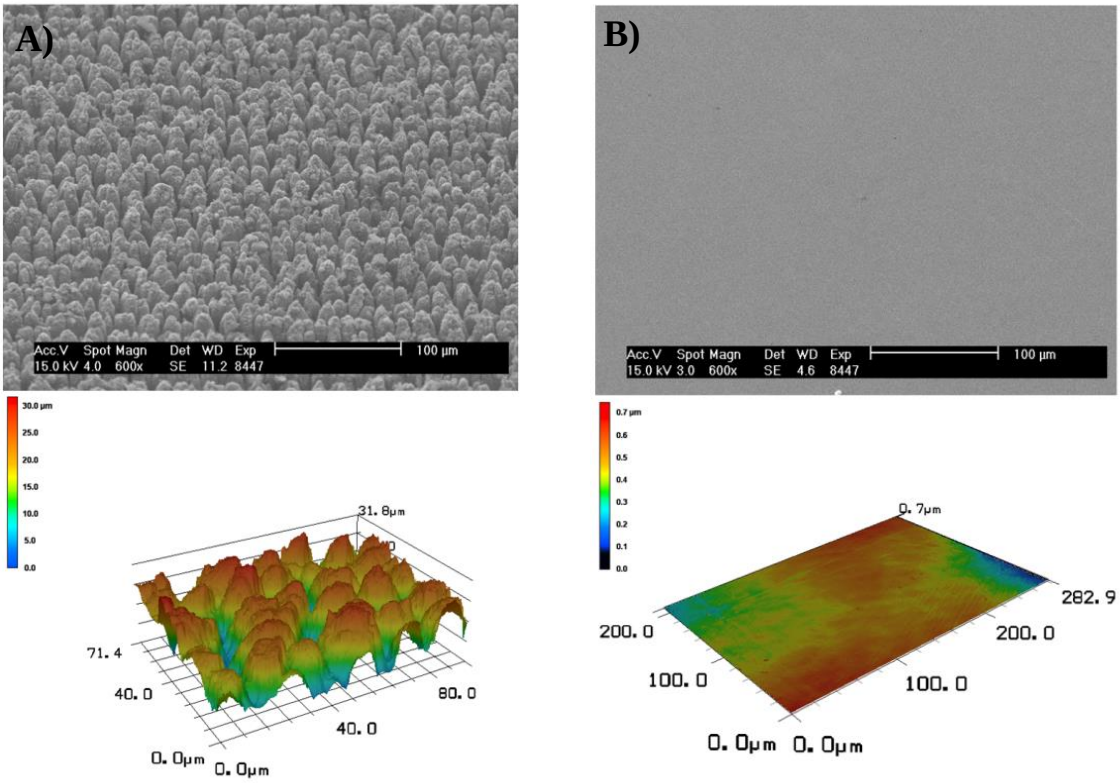

Figure 3-1 SEM images (top) and 3D topology scans (bottom) of (A) ASG-Mounds and (B) mirror polished test samples. SEM images taken at 600x magnification – scale bars are 100 microns. It should be noted that the colors do not correspond on the topology scans. For the ASG-Mounds red represents a height of 30 microns, while the same color represents a height of 0.7 microns on the polished sample.

Measurements were taken at a variety of random locations on each surface and contact angle was found to independent of sample location. For Deionized water on the processed surface, static contact angle was found to be equal to 0°, while the polished sample had a static contact angle of 75°. With HFE 7300DL as the working fluid, the contact angle of the processed surface was again found to be 0°, while the polished sample had a contact angle of 5°. Contact angle measurements were repeated on a weekly basis throughout the duration of testing for both samples. Ambient laboratory temperature

was assumed to be relatively constant (~22˚C) throughout the duration of tests. Because the samples were stored in open air, oxidation and carbon build up caused changes in wettability over time [63]. Over a time period of a few weeks, the contact angles were found to decrease for the polished sample, and increase for the processed sample. However, a 20 minute ultrasonic bath in isopropyl alcohol would completely restore the wettability properties of the samples. More information on this can be found in a previous work of ours [29]. In addition to ultrasonic bath, the surface of the polished sample was often wiped with a Clorox® wipe. Clorox® wipes were used because they contain chloride, which is effective for removing chromium oxide, which forms on the surface of stainless steel. Table 3-1 gives a summary of results from the surface characterizations.

Table 3-1 Measured surface characteristics

		Contact Angle (°)	
Sample	Surface Roughness (μm)	Deionized Water	HFE 7300DL
ASG-Mounds	4.8	0	0
Mirror-Polished	0.04	75	5

3.2 Leidenfrost Experimental Procedures

Similar to a previous work by the coauthors [29], the droplet lifetime method was used to determine the Leidenfrost point of the test surfaces. This method consists of measuring the evaporation time, also referred to as droplet lifetime, of liquid sessile droplets on a heated surface for various surface temperatures. With the droplet lifetime plotted against surface temperature, the Leidenfrost point is defined as the temperature corresponding to the highest evaporation time [13].

Leidenfrost experiments were conducted on two different 304 stainless steel samples, each 64 mm in diameter and 15 mm in thickness. The first sample was polished to a mirror finish by first sanding its surface with 400 grit sandpaper and then polishing it with a buffing compound. The surface was sanded in one direction until all visible marks on the surface were of the same orientation as a result of the sanding. The sample was then rotated and sanding was repeated until all visible scratches were perpendicular to the original orientation. This process was used to ensure complete sanding of the sample surface. Buffing was accomplished with a high speed buffing wheel and Craftsman Emery Cake Buffing Compound. After buffing, the second sample was processed via FLSP. Because a droplet in the Leidenfrost state tends to move around on the surface in a nearly frictionless manner, a conical depression was machined with a 1° slope and a depth of 0.4 mm at the center of each test surface in order to keep the droplet from rolling off the test area. This depression was machined prior to sanding, polishing, or FLSP, and did not have a major effect on any of the aforementioned surface preparation procedures or FLSP results. This was verified with SEM images and 3D profiles of several locations across the sample after processing. The test surfaces were heated through the use of cartridge heaters implanted inside a heating block, made from copper, and which had dimensions of 76 mm in diameter and 100 mm in length. The heating block was heated by five equally spaced 150 Watt cartridge heaters. The cartridge heaters used were 0.375 inches in diameter and 3.5 inches in length and were controlled by a programmable Ramé-Hart temperature controller with a resolution of 0.1 ^{0}C. A standard K-type thermocouple was embedded 0.8 mm below the lowest point on the surface of the samples to provide feedback to the temperature controller. The thermocouple was

calibrated by the vendor (Omega) prior to purchase; thermocouple error was specified as ± 2.2˚C or .75% of the measured temperature, whichever is greater. The controller maintained a nearly constant surface temperature by varying power output to the cartridge heaters. A schematic of the Leidenfrost point experimental setup is shown in Figure 3-2.

To ensure consistent droplet sizes, a Ramé-Hart precision droplet dispensing unit was used. Drop sizes investigated were nominally 1.77, 8.18, and 33.5 µL corresponding to droplet diameters of 1.5, 2.5, and 4.0 mm respectively. During the experiments, room temperature droplets (about 20 °C) were released about 2 mm above the surface of the test samples. To ensure consistent starting conditions (e.g., initial droplet temperature of 20 ºC), the dropper needle was moved away from the test surface while not in use. At surface temperatures just below or above the LFP, the formation of satellites, or smaller droplets, due to splitting and splashing from the original droplet became common upon droplet impact. Only full droplets that did not have significant formation of satellites were considered for measurements. As a result of this condition, droplets in the transition

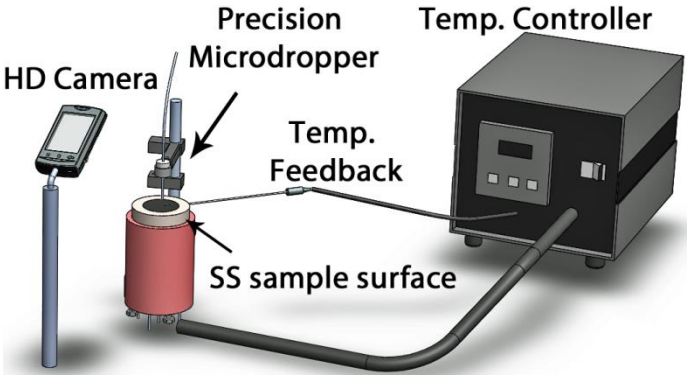

Figure 3-2 Leidenfrost point experimental setup. A precision micro dropper was used in conjunction with a temperature controller to evaporate droplets. Droplets were recorded on a high-definition camera and droplet lifetime was extracted from the video.

boiling regime were almost always excluded. For each droplet size and surface temperature, an average of ten droplet lifetimes was taken.

3.3 Leidenfrost Experimental Results

Figure 3-3 shows the results of the Leidenfrost experiments for Deionized water. The curves are named according to the sample and droplet size investigated (P1.5 represents 1.5 mm droplets on the polished sample; M1.5 represents 1.5 mm droplets on the ASG-Mounds, etc.). The error bars represent the standard deviation of 10 data points for each surface temperature. It should be noted that the error bars tend to be small at temperatures far above the LFP; as surface temperature decreases, the error bars increase to their maximum around the LFP. As indicated on the figure, the LFP is defined as the temperature corresponding to the highest evaporation time. Data points to the left and right of the LFP correspond to droplets in transition and film boiling regimes, respectively. Overall, the LFP on the processed surface is higher than that of the polished surface for all droplet sizes investigated. As for the effects of droplet size, the LFP was shown to shift 40 °C over the range of droplet sizes on the polished sample compared to 100 °C over the same range of droplet sizes on the ASG-Mounds sample. With the smallest droplet size, 1.5 mm, there is a difference of 140 °C between the LFP of the two samples, as seen on Figure 3-3C. This difference increases to 200 °C at the largest droplet diameter of 4.0 mm. This trend shows not only that the Leidenfrost temperature increases with droplet diameter in the case of DI water, but also the rate at which it increases varies from the polished sample to the processed sample. This indicates that the presence of microstructures on the processed surface adds a new interrelated mechanism to the diameter-dependent LFP.

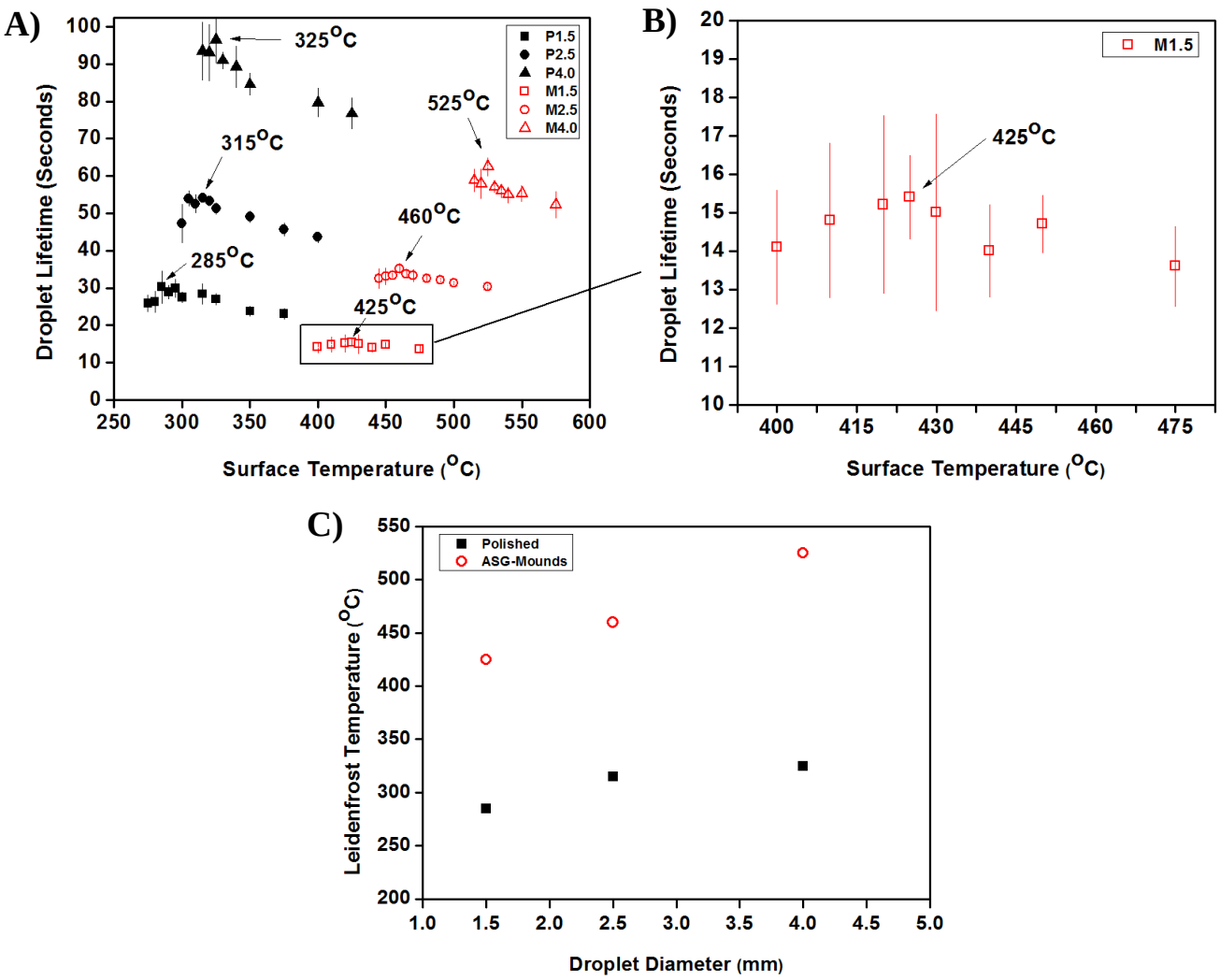

Figure 3-3 Leidenfrost point results using DI water droplets: (A) Droplet lifetime curves of water droplets on polished (black) and FLSP (red) stainless steel test surfaces. (B) Enlarged view of lifetime curve for 1.5 mm droplets on ASG-Mounds. (C) Leidenfrost temperature as a function of droplet diameter shows substantially different rates of change for the mirror-polished and ASG-Mounds samples.

What follows are hypotheses in an attempt to explain the observed results. To this date, a complete and thorough analysis of the Leidenfrost point mechanisms does not exist. Proposed mechanisms in the literature are often simplistic and are tailored to one mechanism while ignoring others. Such approaches are praiseworthy; however, they do not capture the entire physics as to how transition to the Leidenfrost state occurs. The authors believe that transition to Leidenfrost state is a multi-mechanistic phenomenon where all factors are interrelated. This conjugate effect will be illustrated as we try to hypothesize the reasons behind the shifts in the Leidenfrost point from polished to processed surfaces, the effects of the droplet size, and the droplet size dependence of the shifts from a polished to a processed surface.

The Leidenfrost state represents the point of minimum heat transfer therefore it must correspond to the first instance when a stable vapor layer is formed under the entire surface of a sessile droplet. Consider Figure 3-4 which shows a schematic representation

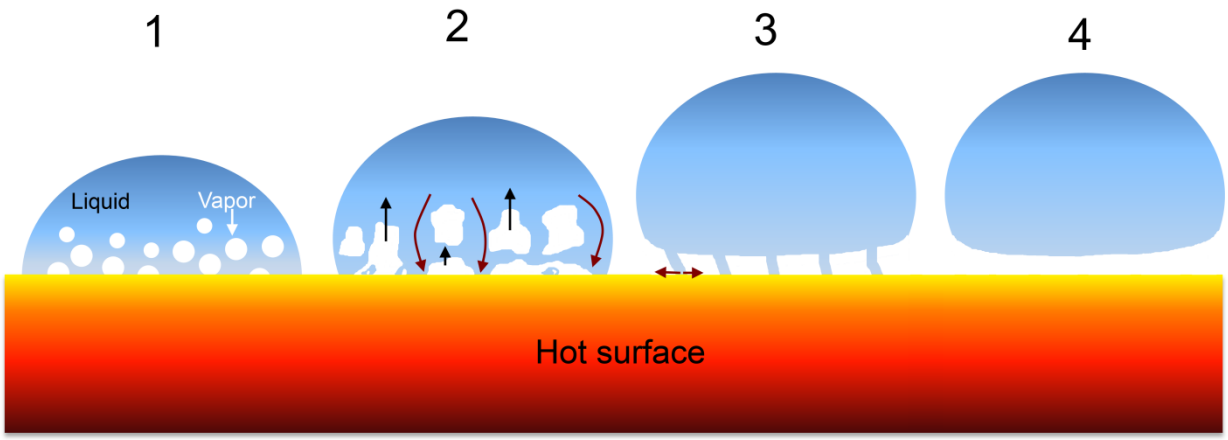

Figure 3-4 Schematic representation of a droplet on a hot surface transitioning to film boiling. (1) Nucleate boiling (2) Coalescence of vapor pockets typically occurs during transition boiling (3) Unstable vapor film just below the Leidenfrost Temperature (4) Film boiling

of the progress towards Leidenfrost state of a droplet on a hot surface. As a result of heat transfer from the surface to the liquid droplet, heterogeneous vapor bubbles form in an unsynchronized fashion based on the availability of active nucleation sites. As heat flux is increased, vapor generation rate and density increase, causing formation of larger vapor pockets on the surface. The prevalence of the formation of these larger vapor pockets is balanced by surface tension forces (quantified through the equilibrium contact angle) and capillary wicking actions, both of which act to promote rewetting. Low contact angle and high capillary wicking action effectively increase the Leidenfrost temperature as observed in the present results (see Fig. 5A). Intermittent contact [29] is another mechanism which can also explain the observed trend. For all cases investigated, the Leidenfrost temperatures of the processed surface are consistently higher than those of the polished surface.

To understand the effects of droplet size on the Leidenfrost temperature, we hypothesize an important condition for the occurrence of the Leidenfrost state. This condition is that the formation of large vapor pockets on the heated surface can only occur if the probability density of synchronous vapor bubble formation (both in space and time) is significantly high enough. The coalescence of two vapor bubbles to form a larger vapor pocket will be impeded if the vapor sites are far from each other or there exists a significant delay in their rate of formation (i.e., while one vapor bubble is just starting to form, its adjacent vapor is in the process of being released). One can argue that the larger the droplet size, the lower the probability density of synchronous vapor bubble formation for a given temperature, hence, the higher the Leidenfrost temperature will be. Furthermore, surfaces that traditionally exhibit exceptional wicking characteristics often

have complex microstructure geometries which can impede escaping vapor. This impedance would increase the probability of vapor bubble coalescence, as it would force the bubbles to remain on the surface longer. It is however expected that at significantly high temperatures (i.e., high heat fluxes), droplet size will stop having effects on the Leidenfrost temperature. We have also noted earlier that the effects of droplet size vary from the polished sample to the processed sample (see Fig. 5C). Droplet size effects seem to be more important in the processed sample than in the polished sample. This is due to the fact that higher droplet size leads to more available surface area for surface tension forces and capillary wicking actions. Hence, high temperatures will be required to overcome the increasingly higher surface forces and capillary wicking with increasing droplet size. Figure 3-5 shows the results of the droplet lifetime measurements for HFE 7300DL. Due to limitations of the precision micro dropper, droplet sizes investigated for

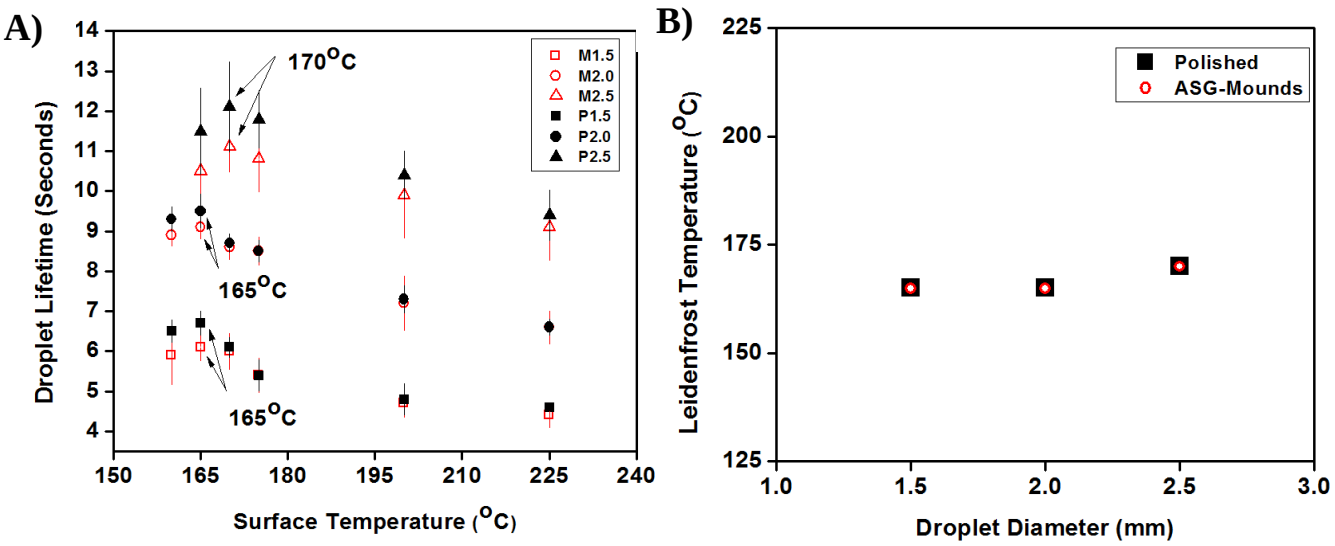

Figure 3-5 (A) Droplet lifetime curves of HFE 7300DL on polished (black) and FLSP (red) stainless steel test surfaces. (B) Leidenfrost temperature as a function of droplet diameter shows that the LFP is the same for both the Mirror-Polished and ASG-Mounds samples. Only minimal shifts in the LFP were observed over the range of droplet sizes.

HFE 7300DL were 1.5, 2.0, and 2.5 millimeters. As can be seen in the figure, Leidenfrost temperatures were nearly the same for both the FLSP and mirror-polished samples at each of the droplet sizes. For the 1.5 and 2.0 mm droplets there was no shift in the LFP (165 °C), while the 2.5 mm droplets displayed a very small increase of LFP (5 °C). Although the LFP was nearly the same for both samples at each of the droplet sizes, droplet lifetimes were smaller on the FLSP sample for each droplet size indicating a more efficient heat transfer from the FLSP surface.

The physics and mechanisms discussed above in the case of DI water also apply for the HFE 7300DL results as well; however the two fluids have different thermophysical properties. The argument stated earlier for the shift of the Leidenfrost temperature from polished to processed surfaces was based on the surface tension forces

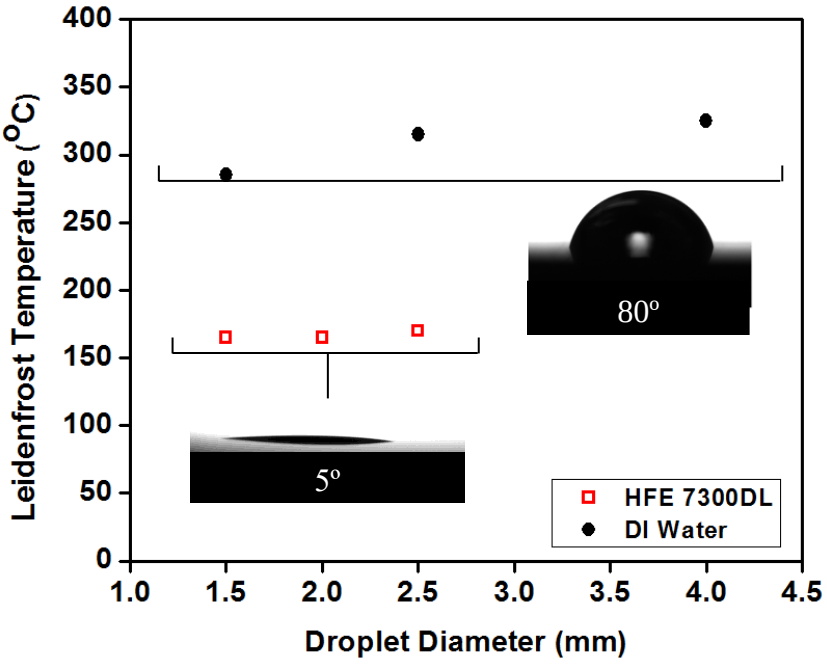

Figure 3-6 Left: Leidenfrost temperature as a function of droplet diameter for both test fluids on the mirror polished sample. Right: Contact angle images for both fluids on the mirror polished surface.

(wettability) and capillary wicking. Even though the surface tension of HFE 7300DL is five times lower than water, it is much more volatile. The HFE's high volatility (i.e., liquid front thin film vaporizes immediately in contact with heated surface) undermines its ability to take advantage of augmented surface area from either larger droplet size or the presence of microstructures. Another important mechanism which may equally play an important role in determining the Leidenfrost temperature is the two-phase hydrodynamics within the sessile droplet. Going back to Figure 3-4(2), large vapor pockets resulting from the combination of vapor bubbles are released from the surface in a form of vapor columns. One can imagine the possibility of a premature Leidenfrost state if the vapor columns are not allowed to escape through the liquid. The viscosity of HFE 7300DL is larger than that of water and considering the viscous forces on the vapor columns, the Leidenfrost temperatures with HFE 7300DL are expected to be relatively lower than those with water. This conclusion agrees with our experimental results as shown in Figure 3-6 summarizes the results of the Leidenfrost experiments. Maximum Delta corresponds to the difference between the 4.0 and 1.5 millimeter droplets for DI water and the 2.5 and 1.5 millimeter droplets for the HFE 7300DL.

Table 3-2 Leidenfrost results

Droplet Diameter (mm)	Leidenfrost Temperature (^{o}C)					
	Deionized Water			HFE 7300DL		
	Mirror-Polished	ASG-Mounds	Delta	Mirror-Polished	ASG-Mounds	Delta
1.5	285	425	140	165	165	0
2.0	*	*	*	165	165	0
2.5	315	460	145	170	170	0
4.0	325	525	200	*	*	*
Maximum Delta	40	100	60	5	5	0

CHAPTER 4

Thermal Stability of Rare Earth Oxide Coated Superhydrophobic Microstructured Metallic Surfaces

Heat treatment experiments were first carried out on a processed microstructured surface due to the possibility of increased hydrocarbon adsorption [64]; the processed sample underwent FLSP, while another was polished to a mirror-finish for control. FLSP creates a quasi-periodic, self-organized, hierarchical surface with micron scale conical structures coated in a fine layer of nanoparticles [54–59].

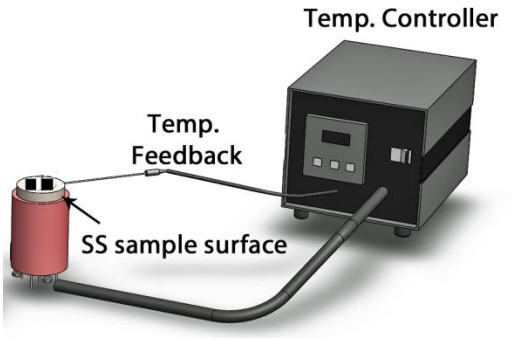

Figure 4-1 Test surface heating block setup.

4.1 Rare Earth Oxide Surface Characterization

Immediately following fabrication, test surfaces were characterized via, X-Ray Diffraction (XRD), Scanning Electron Microscopy (SEM), and contact angle. XRD was performed using a PANalytical Empyrean with Cu K_α radiation. SEM was performed in a FEI Helios 660 operating at 20kV with an EDAX SDD Octane super EDS detector. The samples were then heated via a stainless steel heating block controlled by a programmable Ramé-Hart temperature controller with a resolution of 0.1˚C (Figure 4-1). A thermocouple was embedded just below the surface of the block on which the samples were placed in order to provide feedback to the temperature controller. Samples were

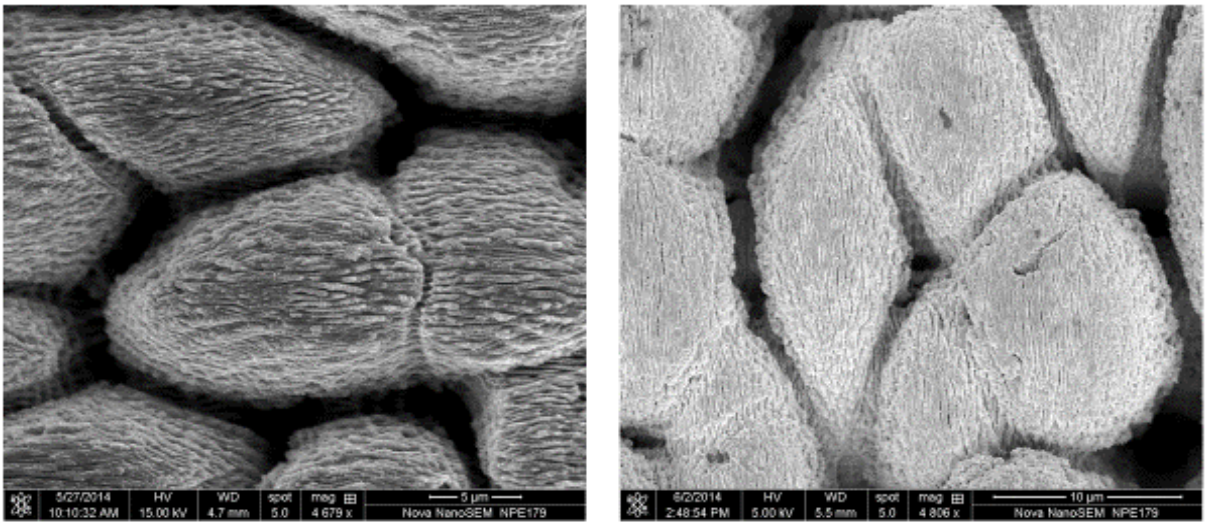

Figure 4-2 Comparison of SEM images before (left; 5 µm bar) and after (right; 10µm bar) deposition.

annealed by temperatures increasing by 20˚C. After each heating cycle the sample was allowed to cool to room temperature and monitored via contact angle and XRD. Figure 4-2 shows SEM images of the FLSP surface before and after ceria deposition. After deposition, ridges on the microstructures appear to be more rounded and tightly packed. Figure 4-3 gives XRD results for the FLSP and polished sample before and after ceria deposition, as well as post heat treatments. The XRD results show there were no phase changes occurring on the surface during heat treatments.

4.2 Results and Discussion

The results of the annealing process on the contact angle of the FLSP and mirror-polished samples can be seen in Figure 4-4(A). The initial contact angles were 133˚ and 95˚ for the processed and smooth (mirror-polished) surfaces, respectively.

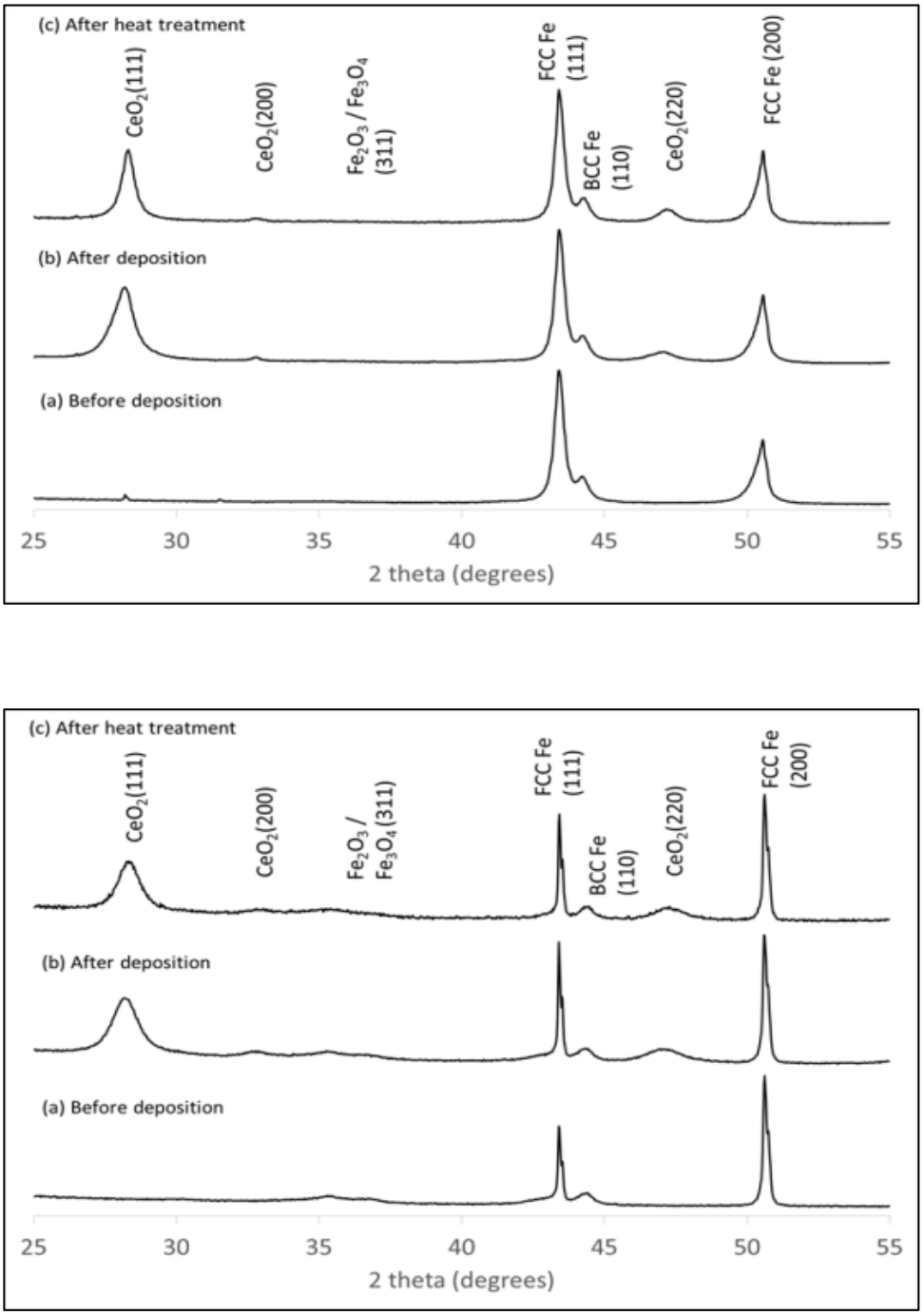

Figure 4-3 XRD spectrum of the mirror-polished (top) and FLSP stainless steel 316 samples coated with 200 nm cerium oxide (a) before deposition, (b) immediately after deposition, and (c) after final heat treatment.

For the FLSP surface, there was a steady increase in hydrophobicity with temperature until approximately 140˚C, at which point there was a rapid decline in the contact angle. The mirror-polished sample showed a similar trend until about 120˚C at which point there was a more gradual decline in the contact angle of the surface. Subsequently, samples were left in laboratory air for one week, over which time hydrophobicity returned to pre-heat-treatment levels. Cleaning the samples with a 20 minute ultrasonic bath in isopropyl alcohol resulted in samples becoming superhydrophilic. It became apparent that REO's are in fact not intrinsically hydrophobic as had been suggested by [50]. Our observations were now in agreement with a study [51] that appeared in the literature while the present study was conducted: samples which had been stored in laboratory air had adsorbed hydrocarbons, a natural process to reduce surface energy. Heating the samples had subsequently caused the hydrocarbons to be removed from the surface [65,66], rendering the samples hydrophilic. It was interesting

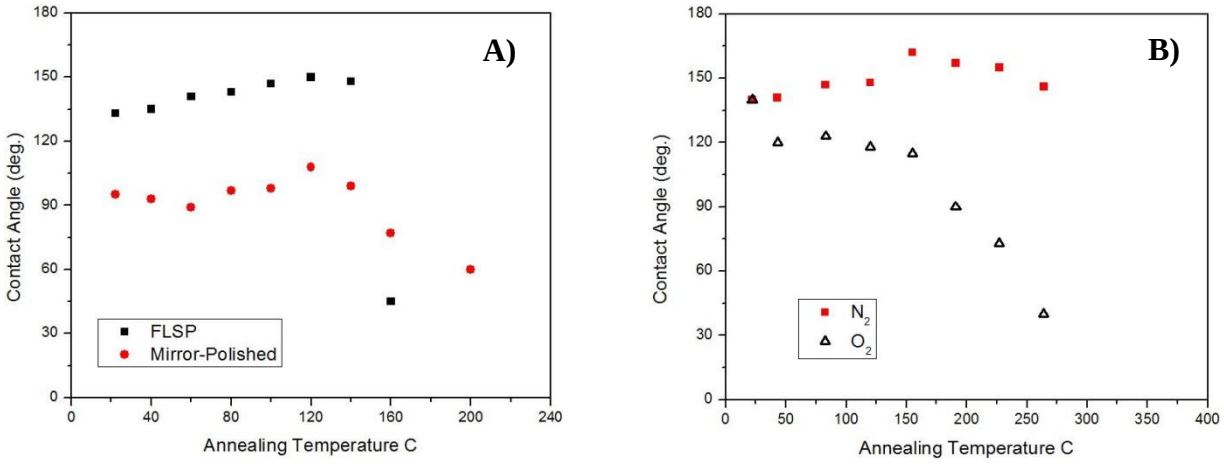

Figure 4-4 A) Contact angle as a function of annealing temperature in ambient air for FLSP and mirror-polished surfaces sputtered with 200nm of Cerium Oxide. B) Effects of gas composition on contact angle as a function of annealing temperature for an FLSP sample sputtered with 200nm of Cerium Oxide.

to note, however, that prior to loss of hydrocarbons, contact angle was increasing with annealing temperature. This suggests that delamination effects may have assisted in roughening the nanostructure thus promoting Cassie-Baxter wetting. Furthermore, post heat treatment, samples showed contact angles lower than the original values on polished stainless steel further indicating that the surfaces did not regress to their original, pre-deposition state.

Subsequently, the samples were stored in laboratory air and allowed to regain hydrophobicity once again. The FLSP sample was then heated in a nitrogen gas heating environment. In order to isolate atmospheric effects during heating, the sample was heated in a Ramé-Hart environmental chamber (Figure 4-5). This chamber had a K-type thermocouple embedded just below the surface, and two evenly-spaced cartridge heaters for heating purposes. The chamber was controlled by the previously mentioned Ramé-Hart temperature controller with 0.1˚C resolution. The thermocouple provided feedback to the controller which maintained the desired temperature by varying output. A small sealable hatch in the top could be opened to deposit drops for contact angle

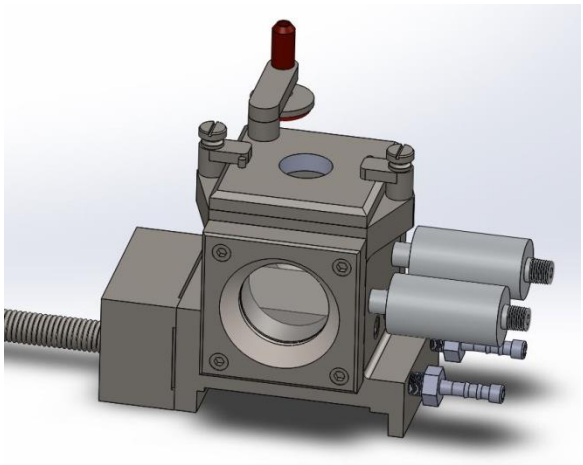

Figure 4-5 Environmental heating chamber.

measurements. The chamber was equipped with flow nozzles such that the device could function as a purge box.

The FLSP sample then underwent the cyclic heat treatment in the controlled environment up to 265˚C due to experimental setup limitations. During heating and contact angle measurement, the chamber was exposed to a flow of nitrogen gas (99.9% purity, Matheson TRIGAS) so as to displace any ambient contaminants. The hose outlet was held beneath water so as to prevent any backflow. After the annealing in nitrogen was complete, the sample was again placed in the laboratory, allowed to regenerate, and placed back into the chamber to repeat the heat treatments. The sample underwent the same heating process, this time exposed to oxygen gas (99.6%, Matheson TRIGAS). As can be seen from Figure 4-4(B), the FLSP surface retained hydrophobicity throughout the duration of the annealing process when it occurred in inert nitrogen whereas hydrophobicity was lost in an oxygen environment. Roughening of a surface can aid adsorption and thus promote stability due to increased surface area [64] which may help explain why the FLSP surface was able to maintain hydrophobicity even when heated to temperatures above ~260˚C, where hydrogen bonds are thought to degrade [65,66]. However, the fact that different results were observed in an oxygen environment suggests the presence of a chemical reaction on the surface. One possible explanation would be oxidation, as new oxidation could facilitate removal of hydrocarbons from the surface. Additionally, new oxidation layers could grow over surface contaminants, blocking them from interacting with water; however, ceria was deposited in the oxidized state (CeO_2), making this explanation less plausible.

After annealing processes were completed, Thermal Gravimetric Analysis (TGA) was performed in order to determine the temperature at which hydrocarbons will be removed from an FLSP surface. Figure 4-6 shows the results of the TGA tests; the horizontal axis represents temperature while the vertical axis represents mass change in milligrams. The blue curve represents a clean FLSP sample being heated to 600˚C and then cooled back to room temperature while the gold curve represents an FLSP sample that has been contaminated with hydrocarbons. As can be seen on the figure, there is almost no change in the curve between heating and cooling for the clean surface, while the contaminated surface experienced mass loss between about 165˚C and 275˚C. This temperature range directly corresponds to temperatures reported in the literature at which hydrogen-carbon bonds will break resulting in lost hydrophobicity on organically contaminated surfaces [65,66]. Cooling the originally contaminated surface back to room temperature did not result in any significant mass gain on the sample indicating that the mass loss was a permanent result of lost hydrocarbons. The temperatures over which

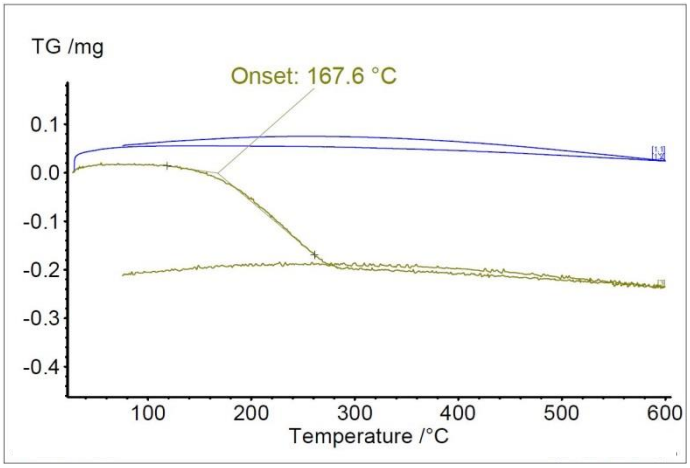

Figure 4-6 TGA results for a superhydrophilic FLSP sample (blue) and a superhydrophobic FLSP sample (gold)

mass loss occurred during TGA are very similar to the temperatures at which the samples shown in Figure 4-4(B) began to lose hydrophobicity, indicating a direct correlation between surface hydrocarbon content and hydrophobicity.

In order to verify the observed atmospheric effects on the thermal stability of REO coatings, two new mirror-polished test surfaces were created in the manner previously described in this paper. After sputtering, the surfaces were placed into a hydrocarbon rich environment to accelerate surface hydrocarbon adsorption. Surfaces were then characterized via EDS prior to any heat treatment. The new test surfaces were heated in the controlled environments used previously on the FLSP surface; one sample was tested in nitrogen the other was tested in oxygen. Figure 4-7 shows the results of annealing test on the mirror-polished CeO_2 surfaces in nitrogen and oxygen. The initial contact angles for the samples were 128˚ and 117˚ respectively; contact angle values are higher than those reported for flat ceria samples [50,51] as a result of increased

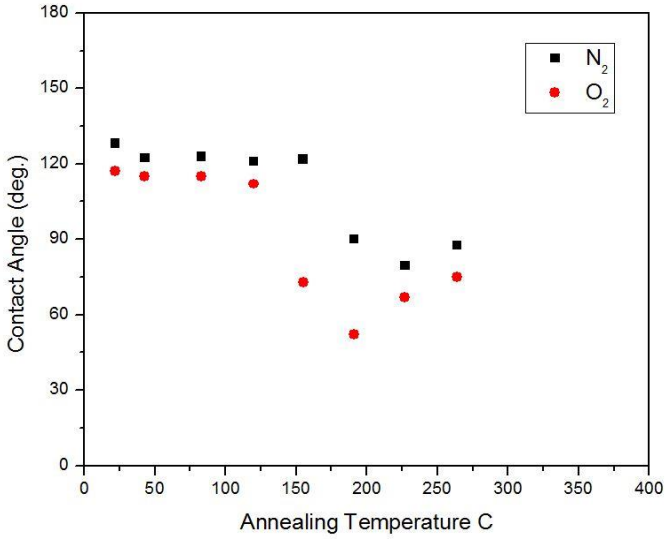

Figure 4-7 Effects of gas composition on the contact angle of mirror-polished stainless steel 310 sputtered with CeO_2 as a function of annealing temperature.

hydrocarbon concentrations. The samples began to lose hydrophobicity at about 150˚C and 190˚C when heated in oxygen and nitrogen respectively. As can be seen on the graph, atmospheric conditions have similar effects on the annealing temperature dependent contact angle for the smooth and FLSP surface though the extent of their effects is different. Loss of hydrophobicity in the oxygen environment occurs at a temperature approximately 40˚C below the temperature of hydrophobicity loss in the nitrogen rich environment. The contact angle dependence on annealing temperature however followed a similar trend for both samples. Table 4-1 shows EDS measurements for the flat ceria samples. Sample 1, heated in nitrogen, showed significant carbon loss as a result of the annealing process, while sample 2, heated in oxygen did not show the same carbon loss. The EDS results for sample 2 did not support our hypothesis on carbon loss; however, it does not reject it either. From the time sample 2 was removed from the heat treatment chamber and placed in the EDS measurement system, carbon adsorption could have occurred. Further work is currently being conducted to understand the fundamental mechanisms at play during the annealing experiments.

Table 4-1 EDS measurements of mirror-polished samples before and after the final heat treatment

	Sample 1		Sample 2	
	Pre Heating	Post Heating	Pre Heating	Post Heating
Carbon	28 ± 3.3	24.7 ± 1.6	22.0 ± 0.2	21.5 ± 0.3
Oxygen	17.2 ± 3.0	18.1 ± 3.0	22.2 ± 1.0	22.8 ± 0.8
Cerium	3.2 ± 1.0	3.4 ± 1.2	5.0 ± 0.3	5.0 ± 0.4

To further investigate the wettability of FLSP surfaces coated with CeO_2, two additional samples were fabricated and allowed to gather hydrocarbons via the previously discussed methods. This time, however, contact angle measurements were modified such that advancing and receding angle data was collected. The advancing and receding angles presented in Figure 4-8 should not be taken as quantitatively accurate, as the samples were only rotated to 45˚ during measurement. A true advancing and receding contact angle would rotate the sample all the way to 90˚ or until the droplet rolled off the surface due to its own weight. However, qualitative data can still be useful. The results of the cyclic heat treatments for two FLSP surfaces coated with CeO_2 can be seen in Figure 4-8; (A) represents the contact angle evolution of the surface heated in N_2 while (B) represents the surface heated in O_2. Originally, the surfaces had similar contact angles; for the sample heated in N_2, the original advancing, receding, and sessile contact angles were 163˚, 138˚, and 158˚, respectively. For the sample heated in O_2, the original angles in the same order were 164˚, 139˚, and 156˚. As shown on the graph, the sample heated in N_2

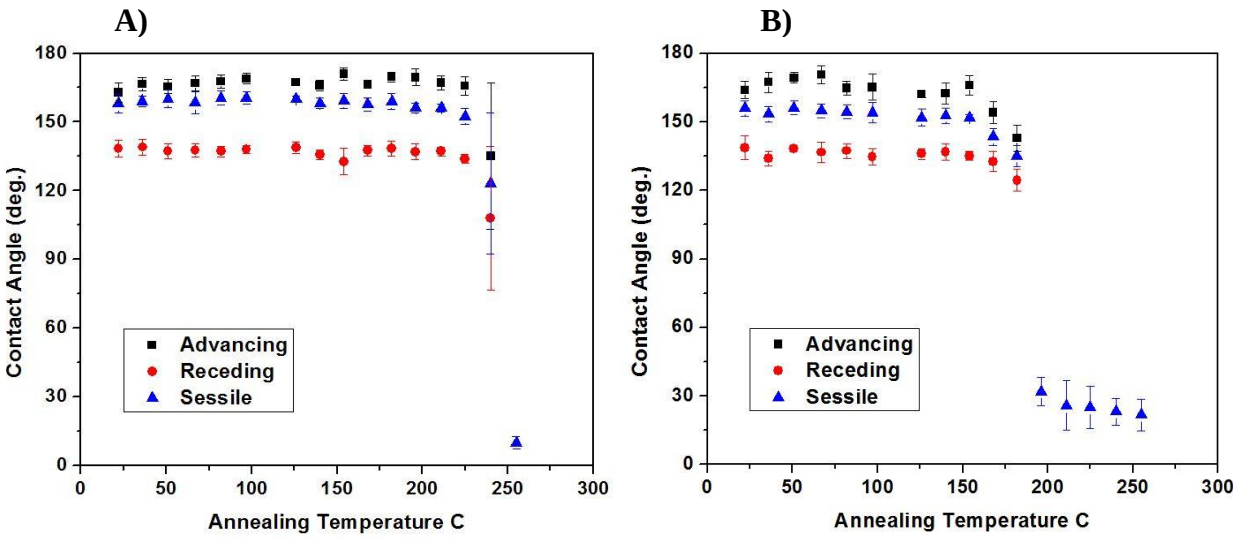

Figure 4-8 Dynamic contact angles for FLSP surfaces heated in Nitrogen (A) and Oxygen (B).

maintained hydrophobicity until approximately 240˚C when hydrophobicity loss first began. After one more heating session at 255˚C, the sample was hydrophilic. For the sample heated in O_2, hydrophobicity loss began at about 168˚C but progressed gradually until about 196˚C when the surface became hydrophilic. EDS measurements for these samples can be seen in Table 4-2. In general, the EDS and contact angle measurements from these samples support the findings presented earlier in this chapter. One important observation to make, however, is the large hysteresis values, or difference between advancing and receding contact angle, shown in Figure 4-8. Contact angle hysteresis values on the order of 30˚ indicate unbalanced forces acting on a droplet as it slides along an incline. Unbalanced forces acting on a droplet are indicative of pinning, a phenomenon where a droplets three-phase sticks to individual microstructures and holds there before jumping to another microstructure rather than smoothly sliding along the surface as would be expected. Pinning, large roll off angles, and large hysteresis values, all suggest that the surface is still very adhesive to droplets. This is not desired in applications where shedding of droplets is a priority, such as condensation.

Table 4-2 EDS measurements of FLSP surfaces before and after heat treatments

	Sample 1		Sample 2	
	Heated in N_2		Heated in O_2	
	After SEM	After Heating	After SEM	After Heating
Carbon	28.51 ± 1.83	24.09 ± 0.95	24.37 ± 2.78	20.61 ± 1.79
Oxygen	43.19 ± 2.39	40.25 ± 1.36	42.61 ± 6.06	43.39 ± 1.11
Cerium	2.83 ± 0.49	3.12 ± 0.28	4.77 ± 0.61	4.74 ± 0.38

CHAPTER 5

Conclusions and Recommendations

5.1 Leidenfrost Conclusions

The effects of droplet size on the Leidenfrost temperature for both polished and processed stainless steel surfaces have been studied using DI water and HFE 7300DL. The stainless steel surface was processed via Femtosecond Laser Surface Processing (FLSP) to form multiscale micro/nanostructures. The Leidenfrost temperatures of the processed surface were consistently higher than those of the polished surface for all droplet sizes in the case of DI water. For the same case, the Leidenfrost temperatures increased with increasing droplet diameter, however the rate at which they increased varies from the polished sample to the processed sample. In the case of HFE 7300DL, the Leidenfrost temperatures were nearly independent of droplet size and completely independent of surface condition under the present experimental conditions. Overall, the Leidenfrost temperatures with HFE 7300DL were lower than with DI water. Observed results from the Leidenfrost experiments have been attributed to a conjugate multi-mechanistic phenomenon which includes effects of surface tension, capillary wicking, droplet characteristic length, two-phase hydrodynamics, and thermophysical properties. This study will be relevant to studies relying on spray quenching for cooling applications.

5.2 Superhydrophobic/Rare Earth Oxide Conclusions

Contrary to the suggestion in [50], this study has shown that rare earth oxides are not inherently superhydrophobic, but in fact their superhydrophobic behavior is attributed to the adsorption of hydrocarbons as suggested in [51]. Additionally, thermal stability of ceria surfaces was investigated and found to depend on ambient heating environment.

Nearly superhydrophobic surfaces were created by roughening a surface via FLSP and deposition of ceria. Subsequent heating resulted in a decrease in contact angle at similar temperatures to the temperature at which hydrocarbons were shown to be removed from metals during TGA analysis. This reduction in hydrocarbons is found to be the reason for the decrease in contact angle as there was no structural change to the ceria layer and EDS measurements showed a decrease in surface carbon content. It was also noted that sample heated in a nitrogen environment showed improved thermal stability over samples heated in oxygen or ambient air, with nearly superhydrophobic properties persisting through heating to about 265˚C. Further experimentation resulted in the creation of flat ceria samples with contact angles significantly higher than those previously reported, due to increased hydrocarbon concentration on the surface. Subsequent annealing of the flat surfaces resulted in a loss of hydrophobicity over the same temperature range suggested by the FLSP surface and TGA analysis confirming that hydrocarbon adsorption is the underlying mechanism for hydrophobicity in rare earth oxide ceramics.

5.3 General Recommendations

This thesis has investigated the potential of FLSP functionalized surfaces for two different classes of applications. The first, the Leidenfrost phenomenon, is relevant to industrial processes that rely on boiling heat transfer for thermal management, often this coiling comes in the form of spray quenching. The results herein suggest that using smaller droplet sizes will be advantageous to the coiling applications. In order to fully understand the physics, however, further work must be done to complete the characterization of heat transfer. In this case, we have used the droplet lifetime method to determine the Leidenfrost Temperature. Other methods exist, and rely on instantaneous

heat transfer during the initial contact (or lack thereof) between the droplet and surface. Such methods would provide better insight into the effects of FLSP for spray quenching applications. Furthermore, this work only determined Leidenfrost Temperature, but not heat flux or total energy removal per droplet. That information would be pivotal in selecting the optimum droplet size for impact. Film boiling should be avoided at all costs, however, under proper working conditions, should also not be a possibility. Therefore, quantities such as heat flux and energy removal will be far more important to the selection of optimum droplet size. From an experimental standpoint, some improvements could be made to improve confidence in the observed results. Due to the nature of FLSP, produced surfaces are highly reactive. Care should be taken to preserve uniform surface parameters between experiments. An inert atmosphere should be used for storage of samples not in use. Additionally, the heating setup for the Leidenfrost experiments could be improved. Currently, the heated surface is open to air and unprotected from random ambient air currents and temperature fluctuations. An enclosed chamber would remedy these potential sources of error.

The second part of this thesis, regarding superhydrophobic rare earth oxide surfaces, is also highly influenced by chemical instability. In this case, however, it was more difficult to determine when a surface was pristine vs when it was contaminated because the contamination was promoting superhydrophobicity. EDS measurements were used to quantify the relative difference in carbon content at various phases of the experiments. However, EDS measurements involve a large interaction volume – we were often measuring bulk material properties rather than true surface properties. As such, the carbon levels measured by EDS are qualitative at best. X-ray photoelectron spectroscopy

(XPS) would be a far more accurate method of measuring surface chemistry. Such systems can be cost prohibitive, but are imperative to truly understanding the chemistry at the surface of a sample. Significant alterations to the test setup were made as discussed in chapter 4; however, some limitation s were still present. The facilities used for sputtering, contact angle, and heating/storage were in a different building that the XRD, SEM, and EDS. This caused non-negligible amounts of time to elapse while the sample was in open air. Furthermore, even after switching to an environmental heating chamber, the sample was not totally isolated from the ambient. This was evidenced by the oxygen sensor data which indicated that significant leaks were present in the chamber. If the chamber was originally filled with nitrogen, over the course of several hours, oxygen levels would often return to about half of atmospheric values. Additionally, the chamber was sealed with polymeric O-rings and Teflon sealing tape, both of which could decompose and deposit low surface energy molecules on the surface during heating. To improve this study, a complete fabrication and analysis bench would be necessary. In such a system, the samples could be processed, characterized, and tested without ever experiencing atmospheric conditions. Alternatively, sample transfer through use of a desiccator could help to mitigate exposure effects.

All of these shortcomings and recommendations aside, one must ask the question, “What are we really studying?” If someone wants to study the fundamental wettability of a surface or material, then extreme care must be taken to preserve the pristine qualities of that surface. On the other hand, if one is more concerned with developing a technology that has potential for industrial application, then it may make more sense to leave the sample in open air and observe how it reacts in a setting that is more similar to how it

will be implemented. Both approaches have value. The former is critical to the development of theory while the latter is imperative to the advancement of technology.

The FLSP technique presented in this thesis results in a large spectrum of tunable surface parameters which show much promise for the enhancement of boiling heat transfer. Additional work is needed to develop durable, superhydrophobic, FLSP surfaces.

REFERENCES

[1] Carey, V. P., 2007, Liquid Vapor Phase Change Phenomena, CRC Press.

[2] Bergman, T. L., Lavine, A. S., Incropera, F. P., and Dewitt, D. P., 2011, Fundamentals of Heat and Mass Transfer, John Wiley & Sons Inc., Hoboken, NJ.

[3] Attinger, D., Frankiewicz, C., Betz, A. R., Schutzius, T. M., Ganguly, R., Das, A., Kim, C. J., and Megaridis, C. M., 2014, "Surface engineering for phase change heat transfer: A review," MRS Energy Sustain., **1**, p. E4.

[4] De Gennes, P. G., Brochard-Wyart, F., and Quere, D., 2013, Capillarity and Wetting Phenomena: drops, bubbles, pearls, waves, Springer Science & Business Media.

[5] Wenzel, R. N., 1949, "Surface Roughness and Contact Angle," J. Phys. Chem., **53**(9), pp. 1466–1467.

[6] Cassie, B. D., and Baxter, S., 1944, "Wettability of Porous Surfaces," Trans. Faraday Soc., (5), pp. 546–551.

[7] Zhang, S., and Gogos, G., 1991, "Film evaporation of a spherical droplet over a hot surface: fluid mechanics and heat/mass transfer analysis," J. Fluid Mech., **222**, pp. 543–563.

[8] Quéré, D., 2013, "Leidenfrost Dynamics," Annu. Rev. Fluid Mech., **45**(1), pp. 197–215.

[9] Avedisian, C. T., and Fatehi, M., 1988, "An experimental study of the Leidenfrost evaporation characteristics of emulsified liquid droplet," Int. J. Heat Mass Transfer, **31**(8), pp. 1587–1603.

[10] Bernardin, J. D., and Mudawar, I., 2002, "A Cavity Activation and Bubble Growth Model of the Leidenfrost Point," J. Heat Transfer, **124**(5), pp. 864–874.

[11] Biance, A. L., Clanet, C., and Quéré, D., 2003, "Leidenfrost drops," Phys. Fluids, **15**(6), pp. 1632–1637.

[12] Bernardin, J. D., and Mudawar, I., 1999, "The Leidenfrost Point : Experimental Study and Assessment of Existing Models," ASME J. Heat Transfer, **121**(4), pp. 894–903.

[13] Tamura, Z., and Tanasawa, Y., 1958, "Evaporation and Combustion of a drop Contacting with a Hot Surface," Seventh Intl Symp. on Combustion, **7**, pp. 509–522.

[14] Baumeister, K. J., Henry, R. E., and Simon, F. F., 1970, "Role of the Surface in the Measurement of the Leidenfrost Temperature," Augment. Convect. Heat Mass Transf. A. E. Bergles R. L. Webb, eds., ASME, New York, pp. 91–101.

[15] Emmerson, G. S., 1975, “The effect of pressure and surface material on the Leidenfrost point of discrete drops of water,” Int. J. Heat Mass Transfer, **18**(3), pp. 381–386.

[16] Xiong, T. Y., and Yuen, M. C., 1991, “Evaporation of a liquid droplet on a hot plate,” Int. J. Heat Mass Transfer, **34**(7), pp. 1881–1894.

[17] Nagai, N., and Nishio, S., 1996, “Leidenfrost temperature on an extremely smooth surface,” Exp. Therm. Fluid Sci., **12**(3), pp. 373–379.

[18] Kim, H., Truong, B., Buongiorno, J., and Hu, L. W., 2011, “On the effect of surface roughness height, wettability, and nanoporosity on Leidenfrost phenomena,” Appl. Phys. Lett., **98**(8), p. 83121.

[19] Vakarelski, I. U., Patankar, N. A., Marston, J. O., Chan, D. Y. C., and Thoroddsen, S. T., 2012, “Stabilization of Leidenfrost vapour layer by textured superhydrophobic surfaces,” Nature, **489**, pp. 274–277.

[20] Hughes, F., 2009, “The evaporation of drops from super-heated nano-engineered surfaces,” Ph.D Thesis, Massachusetts Institute of Technology.

[21] Takata, Y., Hidaka, S., Yamashita, a., and Yamamoto, H., 2004, “Evaporation of water drop on a plasma-irradiated hydrophilic surface,” Int. J. Heat Fluid Flow, **25**(2), pp. 320–328.

[22] Munoz, R. A., and Beving, D., 2005, “Hydrophilic Zeolite Coatings for Improved Heat Transfer,” Ind. Eng. Chem. Res., **44**(12), pp. 4310–4315.

[23] Huang, C. K., and Carey, V. P., 2007, “The effects of dissolved salt on the Leidenfrost transition,” Int. J. Heat Mass Transfer, **50**(1), pp. 269–282.

[24] Bizi-Bandoki, P., Benayoun, S., Valette, S., Beaugiraud, B., and Audouard, E., 2011, “Modifications of roughness and wettability properties of metals induced by femtosecond laser treatment,” Appl. Surf. Sci., **257**(12), pp. 5213–5218.

[25] Wang, Z. K., Zheng, H. Y., and Xia, H. M., 2011, “Femtosecond laser-induced modification of surface wettability of PMMA for fluid separation in microchannels,” Microfluid. Nanofluidics, **10**(1), pp. 225–229.

[26] Avedisian, C. T., and Koplik, J., 1987, “Leidenfrost boiling of methanol droplets on hot porous/ceramic surfaces,” Int. J. Heat Mass Transfer, **30**, pp. 379–393.

[27] Chandra, S., and Avedisian, C. T., 1992, “Observations of droplet impingement on a ceramic porous surface,” Int. J. Heat Mass Transfer, **35**(10), pp. 2377–2388.

[28] Kwon, H., Bird, J. C., and Varanasi, K. K., 2013, “Increasing Leidenfrost point using micro-nano hierarchical surface structures,” Appl. Phys. Lett., **103**, p. 201601.

[29] Kruse, C., Anderson, T., Wilson, C., Zuhlke, C., Alexander, D., Gogos, G., and

Ndao, S., 2013, “Extraordinary shifts of the Leidenfrost temperature from multiscale micro/nanostructured surfaces.,” Langmuir, **29**(31), pp. 9798–9806.

[30] Manzello, S. L., and Yang, J. C., 2002, “An experimental study of high Weber number impact of methoxy-nonafluorobutane C4F9OCH3 (HFE-7100) and n - heptane droplets on a heated solid surface,” Int. J. Heat Mass Transfer, **45**, pp. 3961–3971.

[31] Burton, J. C., Sharpe, A. L., van der Veen, R. C. A., Franco, A., and Nagel, S. R., 2012, “Geometry of the Vapor Layer Under a Leidenfrost Drop,” Phys. Rev. Lett., **109**(7), p. 74301.

[32] Caswell, T. A., 2014, “Dynamics of the vapor layer below a Leidenfrost drop,” Phys. Rev. E, **90**(1), pp. 1–10.

[33] Gottfried, B. S., Lee, C. J., and Bell, K. J., 1966, “The leidenfrost phenomenon: film boiling of liquid droplets on a flat plate,” Int. J. Heat Mass Transfer, **9**, pp. 1167–1188.

[34] Patel, B. M., and Bell, K. J., 1965, “The Leidenfrost phenomenon for extended liquid masses,” Ph.D Thesis, Oklahoma State University.

[35] Nishio, S., and Hirata, M., 1978, “Direct Contact Phenomenon between a Liquid Droplet and High Temperature Solid Surface,” Sixth International Heat Transfer Conference, **1**, pp. 245–250.

[36] Enright, R., Miljkovic, N., Alvarado, J. L., Kim, K., and Rose, J. W., 2014, “Dropwise Condensation on Micro- and Nanostructured Surfaces,” Nanoscale Microscale Thermophys. Eng., **18**(3), pp. 223–250.

[37] Liu, T., and Kim, C. J., 2014, “Repellent surfaces. Turning a surface superrepellent even to completely wetting liquids,” Science (80-.).

[38] Ems, H., and Ndao, S., 2014, “Fabrication of Inverted Trapezoidal Microstructures for Heat Transfer and Microfluidics Applications,” ASME 2014 12th International Conference on Nanochannels, Microchannels, and Minichannels, p. V001T08A001.

[39] Miljkovic, N., Enright, R., Nam, Y., Lopez, K., Dou, N., Sack, J., and Wang, E. N., 2013, “Jumping-droplet-enhanced condensation on scalable superhydrophobic nanostructured surfaces.,” Nano Lett., **13**(1), pp. 179–187.

[40] Ishizaki, T., and Saito, N., 2010, “Rapid formation of a superhydrophobic surface on a magnesium alloy coated with a cerium oxide film by a simple immersion process at room temperature and its chemical stability.,” Langmuir, **26**(12), pp. 9749–9755.

[41] Manoudis, P. N., Tsakalof, A., Karapanagiotis, I., Zuburtikudis, I., and Panayiotou, C., 2009, “Fabrication of super-hydrophobic surfaces for enhanced stone protection,” Surf. Coatings Technol., **203**(10–11), pp. 1322–1328.

[42] Paxson, A. T., Yagüe, J. L., Gleason, K. K., and Varanasi, K. K., 2014, "Stable dropwise condensation for enhancing heat transfer via the initiated chemical vapor deposition (iCVD) of grafted polymer films.," Adv. Mater., **26**(3), pp. 418–423.

[43] Li, Y., Li, L., and Sun, J., 2010, "Bioinspired Self-Healing Superhydrophobic Coatings," Angew. Chemie, **122**(35), pp. 6265–6269.

[44] Wang, H., Xue, Y., Ding, J., Feng, L., Wang, X., and Lin, T., 2011, "Durable, self-healing superhydrophobic and superoleophobic surfaces from fluorinated-decyl polyhedral oligomeric silsesquioxane and hydrolyzed fluorinated alkyl silane.," Angew. Chem. Int. Ed. Engl., **50**(48), pp. 11433–11436.

[45] van der Wal, P., and Steiner, U., 2007, "Super-hydrophobic surfaces made from Teflon," Soft Matter, **3**(4), p. 426.

[46] Guo, Z., Zhou, F., Hao, J., and Liu, W., 2005, "Stable Biomimetic Super-Hydrophobic Engineering Materials," J. Am. Chem. Soc., **157**, pp. 15670–15671.

[47] Erb, R. A., 1964, "Wettability of Metals under Continuous Condensing Conditions," J. Phys. Chem., **2538**(43), pp. 3–6.

[48] Erb, R., 1973, "Dropwise condensation on gold," Gold Bull., **6**(1), pp. 2–6.

[49] Bartell, F. E., and Cardwell, P. H., 1942, "Reproducible Contact Angles on Reproducible Metal Surfaces. I. Contact Angles of Water against Silver and Gold," J. Am. Chem. Soc., **1863**(2), pp. 494–497.

[50] Azimi, G., Dhiman, R., Kwon, H. M., Paxson, A. T., and Varanasi, K. K., 2013, "Hydrophobicity of rare-earth oxide ceramics.," Nat. Mater., **12**(4), pp. 315–320.

[51] Preston, D. J., Miljkovic, N., Sack, J., Enright, R., Queeney, J., and Wang, E. N., 2014, "Effect of hydrocarbon adsorption on the wettability of rare earth oxide ceramics," Appl. Phys. Lett., **105**(1), p. 11601.

[52] Hamilton III, W. J., and Seely, M. K., 1976, "Fog basking by the Namib Desert beetle, Onmacris ungauicularis," Nature, **262**, pp. 774–776.

[53] Parker, A. R., and Lawrence, C. R., 2001, "Water capture by a desert beetle," Br. Commun., **414**(November), pp. 33–34.

[54] Zuhlke, C. A., Anderson, T. P., and Alexander, D. R., 2013, "Formation of Multiscale Surface Structures on Nickel via Above Surface Growth and Below Surface Growth Mechanisms Using Femtosecond Laser Pulses," Opt. Express, **21**(7), pp. 8460–8473.

[55] Zuhlke, C. A., Anderson, T. P., and Alexander, D. R., 2013, "Comparison of the structural and chemical composition of two unique micro/nanostructures produced by femtosecond laser interactions on nickel," Appl. Phys. Lett., **103**(12), p. 121603.

[56] Vorobyev, A. Y., and Guo, C., 2013, “Direct femtosecond laser surface nano/microstructuring and its applications,” Laser Photon. Rev., **7**(3), pp. 385–407.

[57] Nayak, B. K., Gupta, M. C., and Kolasinski, K. W., 2008, “Formation of nano-textured conical microstructures in titanium metal surface by femtosecond laser irradiation,” Appl. Phys. A, **90**(3), pp. 399–402.

[58] Tsibidis, G. D., Stratakis, E., Loukakos, P. A., and Fotakis, C., 2014, “Controlled ultrashort-pulse laser-induced ripple formation on semiconductors,” Appl. Phys. A, **114**(1), pp. 57–68.

[59] Zuhlke, C. A., Anderson, T. P., and Alexander, D. R., 2013, “Fundamentals of layered nanoparticle covered pyramidal structures formed on nickel during femtosecond laser surface interactions,” Appl. Surf. Sci., **283**, pp. 648–653.

[60] Peng, E., Tsubaki, A., Zuhlke, C. A., Wang, M., Bell, R., Lucis, M. J., Anderson, T. P., Alexander, D. R., Gogos, G., and Shield, J. E., 2016, “Experimental explanation of the formation mechanism of surface mound-structures by femtosecond laser on polycrystalline Ni60Nb40,” Appl. Phys. Lett., **108**(3).

[61] LaHaye, N. L., Harilal, S. S., Diwakar, P. K., Hassanein, A., and Kulkarni, P., 2013, “The effect of ultrafast laser wavelength on ablation properties and implications on sample introduction in inductively coupled plasma mass spectrometry,” J. Appl. Phys., **114**(2).

[62] Zuhlke, C. A., Alexander, D. R., Bruce, J. C., Ianno, N. J., Kamler, C. A., and Yang, W., 2010, “Self assembled nanoparticle aggregates from line focused femtosecond laser ablation.,” Opt. Express, **18**(5), pp. 4329–39.

[63] Kietzig, A. M., Hatzikiriakos, S. G., and Englezos, P., 2009, “Patterned superhydrophobic metallic surfaces.,” Langmuir, **25**(8), pp. 4821–4827.

[64] Kwon, H., 2013, “Tailoring hydrodynamics of non-wetting droplets with nano-engineered surfaces,” Massachusetts Institute of Technology.

[65] Cha, S. C., Her, E. K., Ko, T. J., Kim, S. J., Roh, H., Lee, K. R., Oh, K. H., and Moon, M. W., 2013, “Thermal stability of superhydrophobic, nanostructured surfaces.,” J. Colloid Interface Sci., **391**, pp. 152–157.

[66] Tallant, D. R., Parmeter, J. E., Siegal, M. P., and Simpson, R. L., 1995, “The thermal stability of diamond-like carbon,” Diam. Relat. Mater., **4**, pp. 191–199.

APPENDIX

A.1 Leidenfrost Experiment Additional Information

As discussed in chapter 3, the Leidenfrost samples were stored in open laboratory air which led to a change in wettability over time. Due to the conical depression required to keep Leidenfrost droplets on a surface, it was impossible to measure an accurate contact angle. Therefore, wettability change was inspected visually and not quantified. For the processed sample, it was very easy to see if a droplet was no longer wicking completely into the surface; when this occurred, the sample was cleaned with an ultrasonic bath in isopropyl alcohol. On the polished surface, the contact angle could be measured on a flat area of the sample outside the conical depression. Ultrasonic baths were less effective in cleaning the polished surface, and so a Clorox wipe could be used to remove contamination build up if necessary.

The most difficult part of measuring droplet lifetimes is depositing uniform droplets onto the surface. For a droplet to easily fall off of a needle, gravitational forces need to overcome surface tension forces. For a given needle diameter, this corresponds a specific droplet volume. Unfortunately, we wanted to measure droplet lifetimes for droplets of specific diameters, or volumes, so we were not able to test at this golden ratio of volumes that were easily deposited. In order to force droplets off the needle, a sliding stage was used. The stage would be moved up and then downwards towards a stopper where the impact force would cause a momentum difference which allowed droplets to detach. Because the 4mm droplets had to be formed with a much larger needle, they required a much larger impact velocity to detach. As a result of this, droplets were initially impacting the heated surface at very high velocities. Often this resulted in droplet

breakup and the formation of smaller droplets called satellites. Only droplets that did not form satellites were considered for the purpose of measuring lifetimes. Furthermore, if the needle was too close to the surface, the droplets would sometimes jump back up and reattach to the needle. These droplets were also discarded.

Recordings were analyzed via video editing software for the purpose of actually determining droplet lifetimes. The droplet lifetime was said to begin on the first frame in which (near) contact between the droplet and surface can be seen. This was often accompanied by a hissing sound. This hissing sound was likely the result of the droplet actually contacting the surface resulting in rapid boiling. Once the droplet was in a stable film boiling state, no hissing could be heard. The lifetime was said to have ceased on the first frame in which the droplet was no longer identifiable.

A.2 Thermal Stability Experiment Additional Information

As described in chapter 4, experimental observations necessitated a change in the experimental heating setup. Initially, the sample was heated in open atmosphere on the same heating block used for the Leidenfrost experiments. When surface contamination issues were discovered, the samples were moved to an environmental chamber with a flow of either N_2 or O_2 gas during heating. However, this flow was likely causing a temperature offset between where the thermocouple was measuring and the actual surface. To remedy this problem, the flow was turned off such that there was a still environment. This helped to solve the temperature offset issue; however, a new problem arose with the purity of the gas environment. To help understand the magnitude of potential leaks within the system, a zirconium dioxide (ZrO_2) oxygen sensor was added to

the system. Some data from that sensor can be seen in Table A-1 below. Atmospheric O_2 levels are approximately 22%; as can be seen in the table, when the purging gas flow was stopped overnight, the environment in the chamber effectively returned to that of normal laboratory.

Table A-1 Percentage of Oxygen present in environmental chamber environment for a few dates and times

Date (night-morning)	O2% at night	O2% in morning	Gas environment
5/18 - 5/19	96-99	21-26	N_2
5/20 - 5/21	97-100	21-25	N_2
5/22 - 5/26	96-98	18-21	N_2
5/26 - 5/27	0-6	17-22	O_2
5/27 - 5/28	0-3	18-22	O_2
5/28 - 5/29	0-3	18-20	O_2
5/29 - 5/30	0-3	18-22	O_2

Additionally, stricter handling procedures during surface fabrication and characterization were implemented. Samples that were freshly coated with CeO_2 would immediately be tested for contact angle before SEM and EDS analysis. With initial samples, the time exposed to air could be anywhere from a few hours to a few days. With the later samples, the exposed time dropped to a matter of minutes. After SEM/EDS, the samples were placed in the environmental chamber where heating and contact angle measurements were performed. The samples remained in this chamber until testing was finished. However, as discussed previously, this does not mean they were isolated from ambient contaminants.